Rapid evolutionary repair by secondary perturbation of a primary disrupted transcriptional network

Po-Chen Hsu[*] (ID), Yu-Hsuan Cheng[†,‡] (ID), Chia-Wei Liao (ID), Richard Ron R Litan, Yu-Ting Jhou, Florica Jean Ganaden Opoc (ID), Ahmed A A Amine & Jun-Yi Leu (ID)

Abstract

The discrete steps of transcriptional rewiring have been proposed to occur neutrally to ensure steady gene expression under stabilizing selection. A conflict-free switch of a regulon between regulators may require an immediate compensatory evolution to minimize deleterious effects. Here, we perform an evolutionary repair experiment on the *Lachancea kluyveri* yeast *sef1Δ* mutant using a suppressor development strategy. Complete loss of *SEF1* forces cells to initiate a compensatory process for the pleiotropic defects arising from misexpression of TCA cycle genes. Using different selective conditions, we identify two adaptive loss-of-function mutations of *IRA1* and *AZF1*. Subsequent analyses show that Azf1 is a weak transcriptional activator regulated by the Ras1-PKA pathway. Azf1 loss-of-function triggers extensive gene expression changes responsible for compensatory, beneficial, and trade-off phenotypes. The trade-offs can be alleviated by higher cell density. Our results not only indicate that secondary transcriptional perturbation provides rapid and adaptive mechanisms potentially stabilizing the initial stage of transcriptional rewiring but also suggest how genetic polymorphisms of pleiotropic mutations could be maintained in the population.

Introduction

The diversity of biological systems, including transcription regulatory systems, can be a consequence of adaptive evolution (Tenaillon *et al*, 2012), either macroscopically in the body plan (Peter Isabelle & Davidson Eric, 2011) or microscopically at the cellular level (Lynch *et al*, 2014). Altered transcriptional regulation is thought to create phenotypic novelty, thereby playing a crucial role in adaptive evolution and speciation (Carroll, 2000; Wagner & Lynch, 2008; Romero *et al*, 2012; Mack & Nachman, 2017). One particularly intriguing scenario is "transcriptional rewiring," which describes changes to a gene regulatory network across species via *cis* (via polymorphisms in the linked regulatory sequences) or *trans* (through diffusible products of other loci) mechanisms over evolutionary timescales (Scannell & Wolfe, 2004; Dalal & Johnson, 2017). Complete regulon (a group of co-regulated and usually functionally correlated target genes) handover from one TF to another (i.e., TF substitution) is an extreme case of transcriptional rewiring (Li & Johnson, 2010). The rewiring process is often constrained due to the deleterious effects of gene misexpression at intermediate stages, rendering the accumulation of regulatory changes problematic. Nevertheless, stabilizing selection in many species is believed to mitigate such constraints upon encountering new mutations by maintaining appropriate gene expression (Tanay *et al*, 2005; Bedford & Hartl, 2009; Tirosh *et al*, 2009; Goncalves *et al*, 2012; Shi *et al*, 2012; Coolon *et al*, 2014). In other words, extensive *cis-trans* compensation in gene expression underlies transcriptional rewiring (Signor & Nuzhdin, 2018, 2019), potentially enabling "evolutionary tinkering" so that a set of conserved orthologous TFs can be fundamentally repositioned within the regulatory networks of a species (Lavoie *et al*, 2010). A "redundancy" mechanism has been proposed to explain TF substitution, whereby redundant and/or cooperative machinery of regulation underpins rewiring without giving rise to drastic changes in phenotypic output (Wohlbach *et al*, 2009; Johnson, 2017). Interestingly, modeling of genomic data from diverse species supports that the evolution of gene expression best fits the "house-of-cards" model of stabilizing selection, whereby mutations with large phenotypic effects rather than small effects evolutionarily change current transcriptional networks and allow them to be effectively reshuffled to form new networks (Hodgins-Davis *et al*, 2015). However, such large-effect mutations may be a double-edged sword due to their deleterious pleiotropic effects (Dittmar *et al*, 2016). Therefore, we aimed to investigate whether and how compensatory

Institute of Molecular Biology, Academia Sinica, Taipei, Taiwan
*Corresponding author. Tel: +886 2 27899216; E-mail: godshi2006@gmail.com
†Present address: Morgridge Institute for Research, Madison, WI, USA
‡Present address: Howard Hughes Medical Institute, University of Wisconsin-Madison, Madison, WI, USA

evolution works efficiently to deal with this conflict (trade-offs from new large-effect mutations) when the "redundancy" mechanism (redundant and/or cooperative machinery of regulation) is unavailable as new transcriptional networks evolve.

To achieve this goal, we conducted an evolutionary repair experiment. Evolutionary repair is a category of experimental microbial evolution whereby the founder strain contains at least one genetic perturbation (e.g., a single gene deletion; LaBar *et al*, 2020). A general concern for evolutionary repair experiments is whether such a theoretically rare event can in fact happen in nature because a genetic perturbation would be negatively selected in natural populations and thus kept at a low frequency. Therefore, we chose a target gene whose loss of function causes condition-dependent deleterious effects, which generally allows the perturbed founders to persist in a changing environment long enough to evolve a compensatory mutation.

Using the yeast *L. kluyveri* as a model, we first deleted the TF gene *SEF1* involved in respiration and growth (Hsu *et al*, 2021) to create a less-fit founder strain displaying pleiotropic defects (i.e., misregulation of multiple TCA cycle genes that affect respiration-related and -unrelated traits). The *L. kluyveri* Sef1 was chosen due to its known condition-dependent phenotypes, completely characterized direct target genes, simple condition-responsive regulation, and proper evolutionary divergence from the model baker's yeast (Hsu *et al*, 2021). All these advantages will help to simplify subsequent investigation after the evolutionary repair experiments. Complete loss of Sef1 excludes the possibility of "stabilizing" evolution via the "redundancy" mechanism. Then, we performed our evolutionary repair experiment through *sef1Δ* suppressor development to screen for potential large-effect compensatory mutations. We then identified two adaptive loss-of-function mutations of *IRA1* and *AZF1*, respectively, in different selective conditions. We further investigated the pleiotropic effects caused by the *azf1* loss-of-function mutation. We especially demonstrated that misexpression of multiple TCA cycle genes caused by *sef1Δ* can be simultaneously compensated by the *azf1* loss-of-function mutation. Our results demonstrate a process of "quick-and-dirty" compensatory evolution in gene expression following a sudden loss of a TF under specific conditions that precluded a smooth transition via the redundancy mechanism. This potentially mimics the extreme case of the incipient stage of transcriptional rewiring wherein the target genes are disconnected from the primary TF without drastic misexpression, allowing the cells to survive and the perturbed transcriptional network to further evolve.

Results

Evolutionary repair rapidly suppressed the fitness defects caused by *sef1Δ* transcriptional network perturbation

Consistent with our previous work (Hsu *et al*, 2021), the *L. kluyveri sef1Δ* mutant is slightly less fit (slower growing) than *SEF1* strains maintained at normal temperature (28°C) under fermentative conditions [YPD: yeast extract-peptone dextrose (Dex)], with incubation under respiratory conditions [YPGly: yeast extract-peptone glycerol (Gly)] or heat stress (37–39°C) further impairing growth (Fig 1A). The diminished maximal growth rates of the *sef1Δ* mutant

calculated from source growth curves (Appendix Fig S1A and B) under two respiratory conditions (post-diauxic shift and YPGly, Appendix Fig S1C) are shown in Fig 1B. An RNA-seq analysis supports these phenotypic outcomes, showing clear downregulation of multiple TCA cycle genes required for respiratory and optimal fermentative growth (Fig 1C, and Datasets EV1 and EV2).

Interestingly, we noticed that some colonies displaying greater fitness formed among the *sef1Δ* population during the growth assay, especially under the more stringent conditions (YPGly + heat stress). Increasing the incubation time accentuated the outcompeting growth of these fitter cells relative to congeners (Fig 1D), suggesting that selection for suppressors of *sef1Δ* mutant phenotypes may occur rapidly and efficiently. Such adaptive mutations could arise from *de novo* mutations formed after selection or represent low-frequency genetic variants that pre-existed in the founder colony before selection (Teng *et al*, 2013). In terms of this latter, the hypothetical presence of heterogeneous quasi-species founder colonies (Appendix Fig S1D) may accelerate the evolution of cells upon losing *SEF1*, changing their evolutionary trajectories (Appendix Fig S1E). Therefore, we performed a large-scale *sef1Δ* suppressor development experiment (in this study, we also consider it as an evolutionary repair experiment) to investigate how cells evolve to deal with the loss of the transcriptional hub *SEF1* that affects multiple downstream fitness-contributing genes.

First, we created the *sef1Δ* and then the *sef1Δchs3Δ* (tetrad dissection-competent) lines from the wild-type MATa strain, before performing a mating-type switch to obtain a MATα strain (Appendix Fig S2A). Two independent suppressor development experiments were performed by plating 10^8 MATa and MATα founder cells on YPGly plates at 28–39°C for 8 days (Appendix Fig S2B, step A). During that process, larger suppressor colonies carrying the correct drug markers were picked (Appendix Fig S2C, steps A, B, and C). Finally, a total of 240 *sef1Δ* suppressors were isolated, including 144 MATa lines and 96 MATα lines that evolved at different temperatures (Appendix Fig S3A). To characterize the adaptive effects of each clone, we evaluated their fitness by comparing their growth patterns on agar plates against two reference strains (the wild-type and the corresponding *sef1Δ* founder), and then assigned a simple fitness score under YPD and YPGly conditions based on fitness categories (Appendix Fig S3B, left and middle columns, with two examples shown in Appendix Fig S3C). The simple fitness scores of all 240 clones are shown in Dataset EV3. To visualize global fitness patterns among the different groups of suppressor clones, we averaged the simple fitness scores and highlighted them with different colors according to the range of mean scores (Appendix Fig S3B, right column, and summarized in Appendix Fig S3D and E). In general, the *sef1Δ* suppressor selected at 28°C (hereafter, 28°C-Evo) displayed more improved fitness than the *sef1Δ* founder under both YPD and YPGly conditions, irrespective of temperature. Hereafter, we describe the 28°C-Evo clones as "double-compensation." In contrast, the *sef1Δ* suppressors selected under heat-stressed conditions (hereafter, 37-, 38-, or 39°C-Evo) showed more improved fitness compared to the *sef1Δ* founder only under YPGly conditions and especially under higher temperatures. Moreover, the 37, 38, and 39°C-Evo clones showed a severe growth defect relative to the *sef1Δ* founder when grown under heat-stressed YPD conditions. We specifically describe these heat-stressed 37-, 38-, and 39°C-Evo clones as "Dex-trade-off and Gly-compensation" hereafter. Only 30 of the 240 (12.5%)
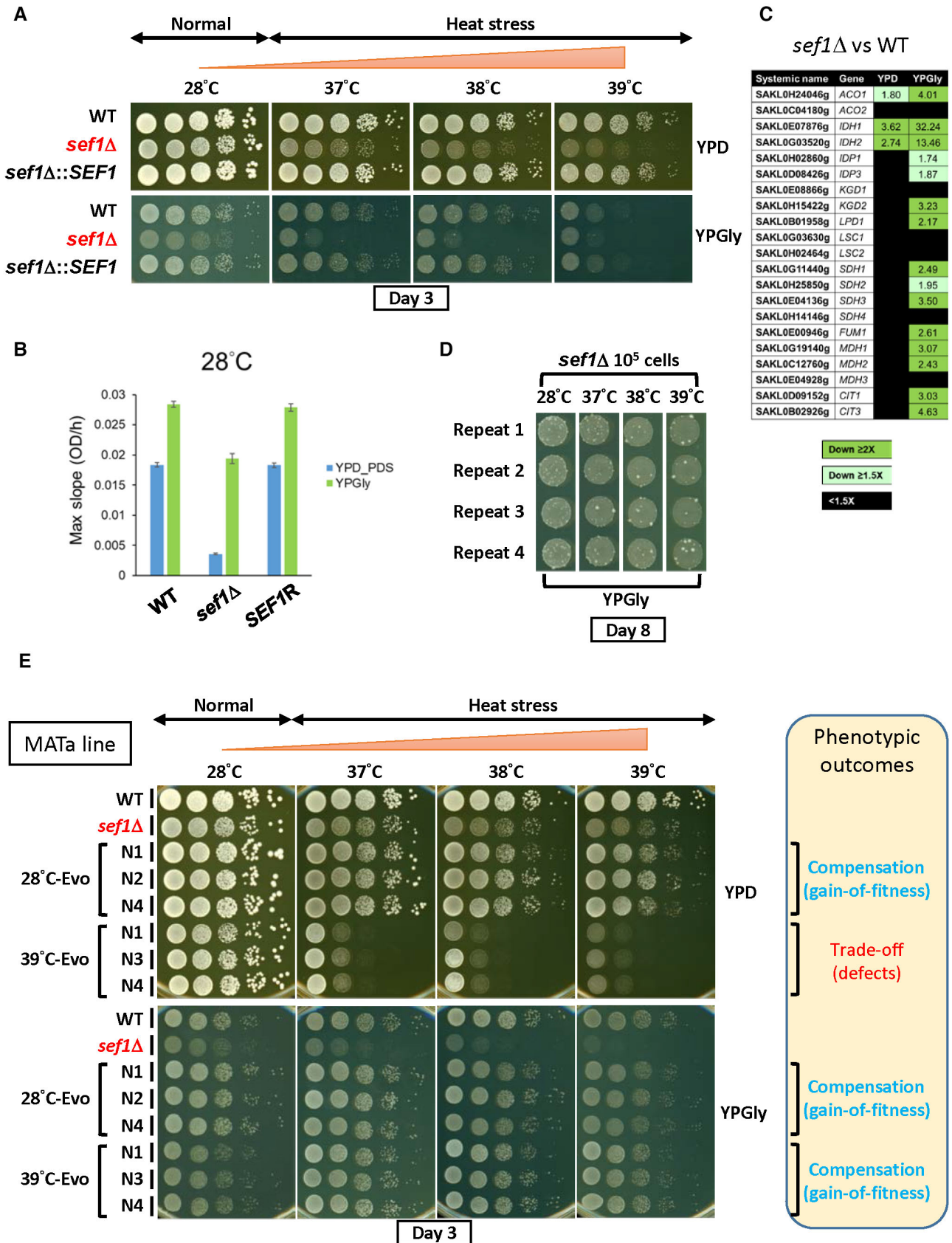
A

B

C

*sef1*Δ vs WT

Systemic name	Gene	YPD	YPGly
SAKL0H24046g	ACO1	1.80	4.01
SAKL0C04180g	ACO2		
SAKL0E07876g	IDH1	3.62	32.24
SAKL0G03520g	IDH2	2.74	13.46
SAKL0H02860g	IDP1		1.74
SAKL0D08426g	IDP3		1.87
SAKL0E08866g	KGD1		
SAKL0H15422g	KGD2		3.23
SAKL0B01958g	LPD1		2.17
SAKL0G03630g	LSC1		
SAKL0H02464g	LSC2		
SAKL0G11440g	SDH1		2.49
SAKL0H25850g	SDH2		1.95
SAKL0E04136g	SDH3		3.50
SAKL0H14146g	SDH4		
SAKL0E00946g	FUM1		2.61
SAKL0G19140g	MDH1		3.07
SAKL0C12760g	MDH2		2.43
SAKL0E04928g	MDH3		
SAKL0D09152g	CIT1		3.03
SAKL0B02926g	CIT3		4.63

Down ≥2X
Down ≥1.5X
<1.5X

D

E

Figure 1.

◄   **Figure 1.   Rapid suppressor development of the *sef1Δ* mutant.**

A   Growth of the *sef1Δ* mutant in response to YPD, YPGly, and heat stress. All plates were incubated for 3 days.
B   The maximal slope growth rate (OD_{600}/h) of the *sef1Δ* mutant in liquid cultures. The growth curves were measured at 28°C by using a Tecan plate reader with intermittent shaking. Results are displayed as average max slopes ± standard deviations (SD) from three technical repeats. YPD_PDS: YPD culture grown to post-diauxic shift phase. "*SEF1*R" indicates the reconstituted strain *sef1Δ::SEF1*.
C   Differential expression of TCA cycle genes in response to *sef1Δ*. The RNA expression profiles from *L. kluyveri* wild-type and *sef1Δ* cells grown to early log-phase under both YPD and YPGly conditions are compared. A total of 21 annotated TCA cycle genes are listed, 18 of which are direct targets of Sef1 and the remaining 3 (*IDP1*, *MDH3*, and *CIT3*) are not (Hsu *et al*, 2021).
D   Rapid formation of spontaneous suppressors of *sef1Δ* phenotypes. The *sef1Δ* cells were spotted on YPGly plates at a density of 10^5 CFU/5 μl spot and incubated at the indicated temperatures for 8 days. Cells of ancestral fitness were grown as a background lawn, while the suppressor clones were grown as bigger colonies.
E   The adaptive growth phenotypes of re-purified *sef1Δ* suppressor clones (28°C- and 39°C-Evo, MATa line).

suppressor clones showed inconsistent phenotypic patterns (Appendix Fig S3F), indicating that both the "double-compensation" and "Dex-trade-off and Gly-compensation" phenotypes are quite representative, implying that at least two major trajectories underlie the rapid evolutionary repair response to *SEF1* deletion.

Adaptive phenotypes are monogenically induced by loss-of-function *azf1* or *ira1* mutations

To identify the causal mutations giving rise to the evolved phenotypes, we repurified the suppressor clones from −80°C stocks and confirmed both the "double-compensation" and "Dex-trade-off and Gly-compensation" phenotypes for two independent MATa and MATα lines (Fig 1E and Appendix Fig S4A). Notably, the randomly picked 37°C-Evo and 38°C-Evo clones showed the same pattern of evolved phenotypes as the 39°C-Evo clones did (Appendix Fig S4B), implying that they may carry the same mutations or mutations eliciting similar suppressive mechanisms. Therefore, only three clones each of 28°C-Evo MATa, 28°C-Evo MATα, 39°C-Evo MATa, and 39°C-Evo MATα lines were re-stocked, denoted "N" as indicated in Fig 1E and Appendix Fig S4A, and then subjected to whole-genome sequencing.

By comparing the resulting genomes with those of their ancestors (i.e., the founder strains), we identified mutated loci in all three clones from the two independent lines (MATa and MATα; Dataset EV4, and Fig 2A and B). Interestingly, only two (*IRA1* and *FLO1*) and four (*FLO1*, *AZF1*, SAKL0D15356pg, and *AMD2*) loci were shared among the respective 28°C-Evo and 39°C-Evo lines. The allele frequencies of the *FLO1* and *AMD2* mutations are < 100% and quite diverse between clones, and SAKL0D15356pg is a pseudogene. Subsequent examination of mutation types revealed that 28°C-Evo lines carry deletion, missense, or loss-of-function (premature stop codon-gained) mutations in the *IRA1* loci (Fig 2C) and 39°C-Evo lines carry missense and another type of loss-of-function mutations (frameshift) in the *AZF1* loci (Fig 2D), supporting that *ira1* and *azf1* loss-of-function alleles are the causal mutations in the 28°C-Evo and 39°C-Evo suppressors, respectively.

To prove that the adaptive phenotypes are monogenic, we performed tetrad dissection analyses by backcrossing the MATa suppressor clones with their MATα founders. We checked three for each of the MATa 28°C-Evo and MATa 39°C-Evo clones. After sporulation, one tetrad of each mating pair was dissected. All four spores of each tetrad were phenotyped and the candidate causal mutation loci were sequenced. All tetrads showed a perfect 2-to-2 ratio between adaptive versus wild-type phenotypes, consistent with the

2-to-2 genotypes (Appendix Figs S5A–C and S6A–C), indicating a clear monogenic effect of the adaptive mutation. As expected, deletion of *IRA1* or *AZF1* alone in the parental *sef1Δ* strains proved sufficient to phenocopy the 28°C-Evo and 39°C-Evo suppressors, respectively (Fig 2E and F).

To estimate the overall frequency of *azf1* loss-of-function mutations and occurrence of the "Dex-trade-off and Gly-compensation" phenotypes, we Sanger sequenced the *AZF1* loci of 30 more randomly picked heat stress-evolved *sef1Δ* suppressors in both MATa and MATα lines (Fig EV1A and B). In combination with the aforementioned six whole genome-sequenced clones, about 83.33% (30/36) of them carried *azf1* mutations, including 15 premature stop codon-gained, 11 frame-shifted, and four missense mutations. The higher proportion of premature stop codon-gained and frame-shifted mutations suggests that *azf1* loss-of-function mutations are the major causal mutations in this batch of suppressors. Moreover, about 85.26% (133/156) of the total heat stress-evolved *sef1Δ* suppressors displayed clear "Dex-trade-off" phenotypes (Fig EV1C and Appendix Fig S3E), slightly higher than the estimated *azf1* frequency (83.33%). This finding indicates the presence of non-*azf1* mutations which also result in the "Dex-trade-off and Gly-compensation" phenotypes (Fig EV1B).

Similarly, the overall frequency of *ira1* loss-of-function mutations was estimated by Sanger sequencing for the *IRA1* loci of 10 more randomly picked 28°C-evolved *sef1Δ* suppressors in both MATa and MATα lines (Fig EV2A and B). In combination with the aforementioned six whole-genome-sequenced clones, about 75% (12/16) of them carried *ira1* mutations, including only three premature stop codon-gained, one frame-shifted, four in-frame deletion, and four missense mutations. It is hard to determine the mutation functionalities simply by the mutation types. Therefore, we used qualitative desiccation sensitivity (shown as post-desiccation viability) to represent the severity of *ira1* loss-of-function mutations or other mutations generating the same effect as *ira1* loss-of-function does (Ratnakumar *et al*, 2011; Welch *et al*, 2013). As shown in the control assays, the *ira1Δ* mutations were hypersensitive to desiccation in both wild-type and *sef1Δ* backgrounds and the negative control *azf1Δ* strains were not (Fig EV2C). The loss-of-function and hypomorphic *ira1* mutations were also distinguishable (Fig EV2D). About 92.86% (78/84) of the total 28°C-evolved *sef1Δ* suppressors displayed clear "desiccation hypersensitivity" phenotypes (Fig EV2E), higher than the estimated *ira1* frequency (75%). This finding also indicates the presence of non-*ira1* mutations which cause the "desiccation hypersensitivity" phenotypes in this batch of suppressors (Fig EV2B).
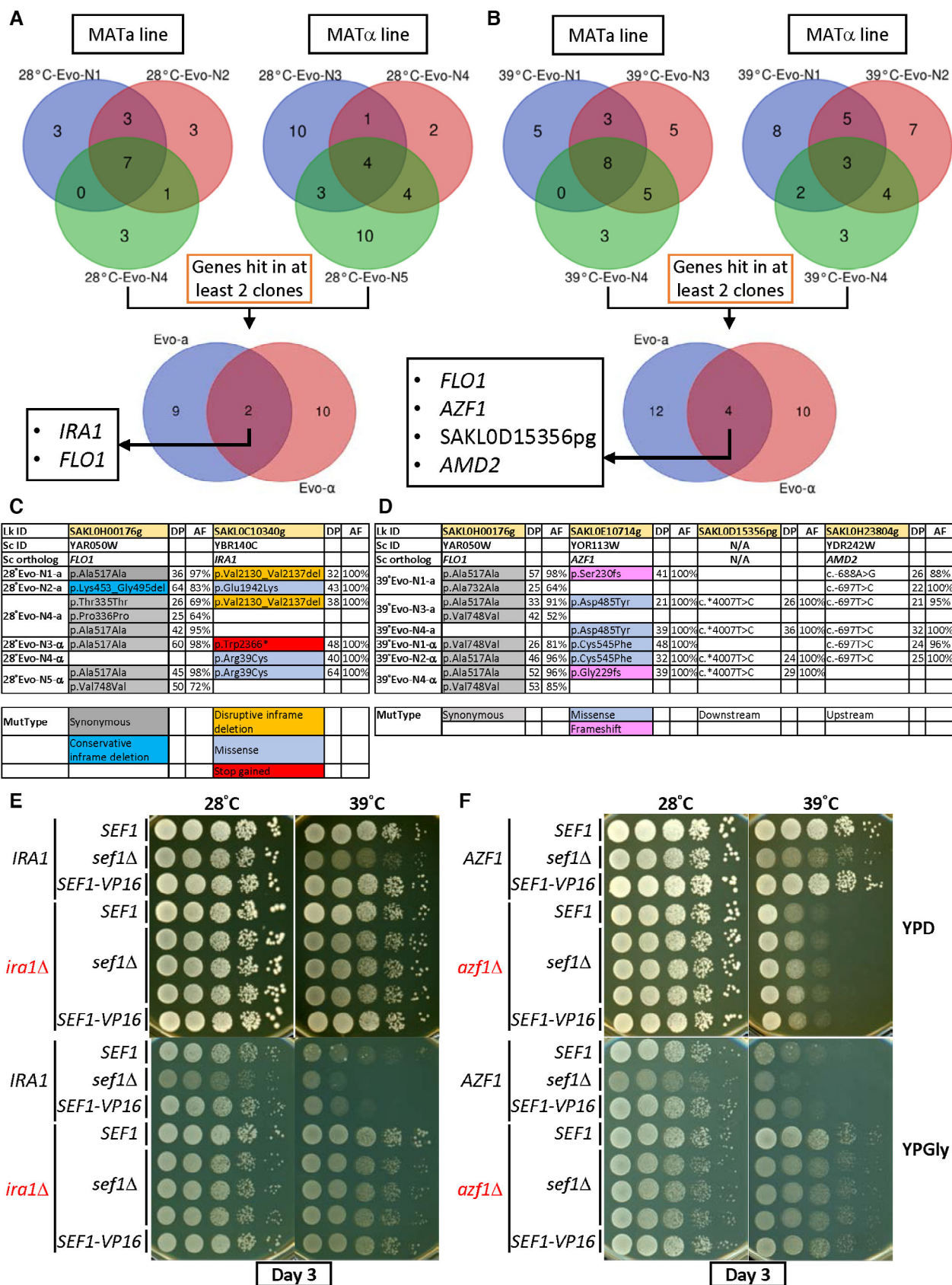
Figure 2.

◀ **Figure 2. Identification of causal adaptive mutations of *sef1Δ* phenotypes.**

A   Convergent mutations among 28°C-Evo *sef1Δ* suppressors between the MATa and MATα lines.

B   Convergent mutations among 39°C-Evo *sef1Δ* suppressors between the MATa and MATα lines.

C, D   Types of candidate causal mutations in (C) 28°C-Evo *sef1Δ* suppressors and (D) 39°C-Evo *sef1Δ* suppressors. DP, read depth; AF, allele frequency. The mutant types (MutType) are highlighted with different background colors.

E, F   (E) The adaptive growth phenotypes of re-constructed *sef1Δira1Δ* strains. (F) The adaptive growth phenotypes of re-constructed *sef1Δazf1Δ* strains. Three independent *sef1Δira1Δ* and *sef1Δazf1Δ* clones were tested. *SEF1-VP16* represents the high-activity *SEF1* strain created by fusing the strong viral transcriptional activator VP16 to the C-terminal of *SEF1* as described (Hsu *et al*, 2021), and one clone for each scenario is shown. *SEF1-VP16* was used to test whether higher Sef1 activity may mask the effect of *azf1Δ* to examine the epistatic relationship.

Sef1, Ira1, and Azf1 belong to related functional modules

Given general concepts of "modular epistasis" among members in an interaction network (Segrè *et al*, 2005) and that suppressive interactions (query and modifier mutations) tend to connect functionally related genes (van Leeuwen *et al*, 2016), we hypothesized that Sef1, Ira1, and Azf1 may be associated with related functional modules. The *L. kluyveri IRA1* is homologous to a negative regulator of the Ras signaling pathway in *Saccharomyces cerevisiae* (Tanaka *et al*, 1990), which is generally coupled with the cAMP-PKA pathway that is activated in response to nutrients and the environment and is responsible for regulating metabolism, cell growth, stress resistance, and glucose adaptation (Conrad *et al*, 2014). *L. kluyveri* Sef1 is a transcriptional activator (Hsu *et al*, 2021), whereas Azf1 is a predicted TF based on orthology to *S. cerevisiae* Azf1 (Stein *et al*, 1998; Slattery *et al*, 2006). We speculated that Ras1-Ira1-cAMP-PKA represents the regulatory signaling pathway upstream of Sef1 and Azf1, so we used either chromosome-integrated or plasmid-based one-hybrid assays (Fig 3A) to evaluate the transcriptional activity of Sef1 and Azf1 in response to Ras1-Ira1-cAMP-PKA pathway signaling. We adopted five Ras1-Ira1-cAMP-PKA hyperactive mutants for this experiment, namely *ira1Δ* (loss of a Ras1-negative regulator), *RAS1*^{G20V} (a hyperactive GTP-bound Ras1 mutant orthologous to *S. cerevisiae RAS2*^{G19V}; Toda *et al*, 1985), *pde2Δ* and *pde1Δpde2Δ* (major loss-of-function mutants of high-affinity cyclic AMP phosphodiesterase), and *bcy1Δ* (loss of the cAMP-dependent protein kinase A inhibitor subunit). As shown in Fig 3B and C, hyperactivation of the Ras1-Ira1-cAMP-PKA pathway modulated Sef1 activity by repressing it under the YPD condition and activating it under the YPGly condition. The changes in Sef1 protein abundance in response to *ira1Δ* were consistent with altered activity (Fig 3D), implying that the underlying regulatory mechanism operates via protein expression or stability.

Next, we investigated Azf1 according to the same strategy described above, which demonstrated that *L. kluyveri* Azf1 is a weak transcriptional activator (Fig 3E). Interestingly, hyperactivation of the Ras1-Ira1-cAMP-PKA pathway modulated Azf1 activity in the same way as observed for Sef1 (Fig 3F and G). However, repression of Azf1 activity under the YPD condition was not detected when we used the chromosome-integrated one-hybrid constructs (i.e., in which the native promoter was used to express Azf1 fused with C-terminal lexA; Fig 3H), and altered Azf1 activity could not be simply explained by changes in protein abundance (Fig 3I). These results imply that Azf1 is regulated by a different and more complex Ras1-Ira1-cAMP-PKA pathway-mediated mechanism than Sef1 (Fig 3J).

Trade-off effects of the loss-of-function *azf1* mutation

Mutations of *IRA1* and its homologs, as well as for members of the entire Ras1-PKA pathway, have been identified previously as adaptive hotspots in numerous experimental evolution and suppressor development studies (Kao & Sherlock, 2008; Parts *et al*, 2011; Wenger *et al*, 2011; Kvitek & Sherlock, 2013; Lang *et al*, 2013; van Leeuwen *et al*, 2016; Venkataram *et al*, 2016; Huang *et al*, 2018; Li *et al*, 2018; Gorter de Vries *et al*, 2019; Kinsler *et al*, 2020; Amine *et al*, 2021; Johnson *et al*, 2021). Moreover, some arguments suggest that they typically emerge as a response to conditions that involve changes in nutrient abundance, such as leading to uncontrolled cell growth in the absence of glucose (Cazzanelli *et al*, 2018). Therefore, we chose to focus on the *azf1* mutation, the "Dex-trade-off and Gly-compensation" effect, which has not been characterized previously.

To identify the genes regulated by Azf1, first, we confirmed that heat stress did not drastically alter the steady-state transcriptional activity of Azf1 (Appendix Fig S7A) but only reduced the abundance of Azf1 proteins (Appendix Fig S7B). Accordingly, deletion of *AZF1* may trigger responses similar to those observed in cells suffering heat stress. For simplicity, we decided to compare RNA expression profiles directly under the normal temperature (28°C) to reduce profile complexity as much as possible. We undertook five comparisons—*sef1Δ*/wild-type, *azf1Δ*/wild-type, *sef1Δazf1Δ*/wild-type, *sef1Δazf1Δ*/*azf1Δ*, and *sef1Δazf1Δ*/*sef1Δ*—and differential gene expression for each as summarized in Appendix Fig S7C–G. Detailed profiles and gene ontology (GO) analyses are presented in Datasets EV1, EV2, and EV5–EV12. In general, we found that the *sef1Δ* mutation affects fewer genes (Appendix Fig S7C and F) than the *azf1Δ* mutation does (Appendix Fig S7D, E, and G).

To further link altered gene expression with *azf1Δ*-induced phenotypic outcomes, we simplified the enriched GO terms by classifying them as *sef1Δ* driven (*sef1Δ*/wild-type and *sef1Δazf1Δ*/*azf1Δ*) or *azf1Δ* driven (*azf1Δ*/wild-type, *sef1Δazf1Δ*/wild-type, and *sef1Δazf1Δ*/*sef1Δ*). As shown in Fig 4A, under the YPD condition, the *azf1Δ*-driven group displays a consistent pattern for enriched GO terms for downregulation of the carbohydrate metabolic process, fatty acid metabolic process, alpha-amino acid metabolic process, and phosphorus metabolic process. In contrast, the *sef1Δ*-driven group only displays consistent enrichment for GO terms relating to downregulation of the isocitrate metabolic process and the TCA cycle. We speculated that the "Dex-trade-off" effect of *azf1Δ* may be attributable to this downregulation. The GO term "carbohydrate metabolic process" of the *azf1Δ*-driven group encompasses 80 downregulated genes, including those about core glucose utilization pathways and especially glycolysis (Appendix Fig S8), indicating
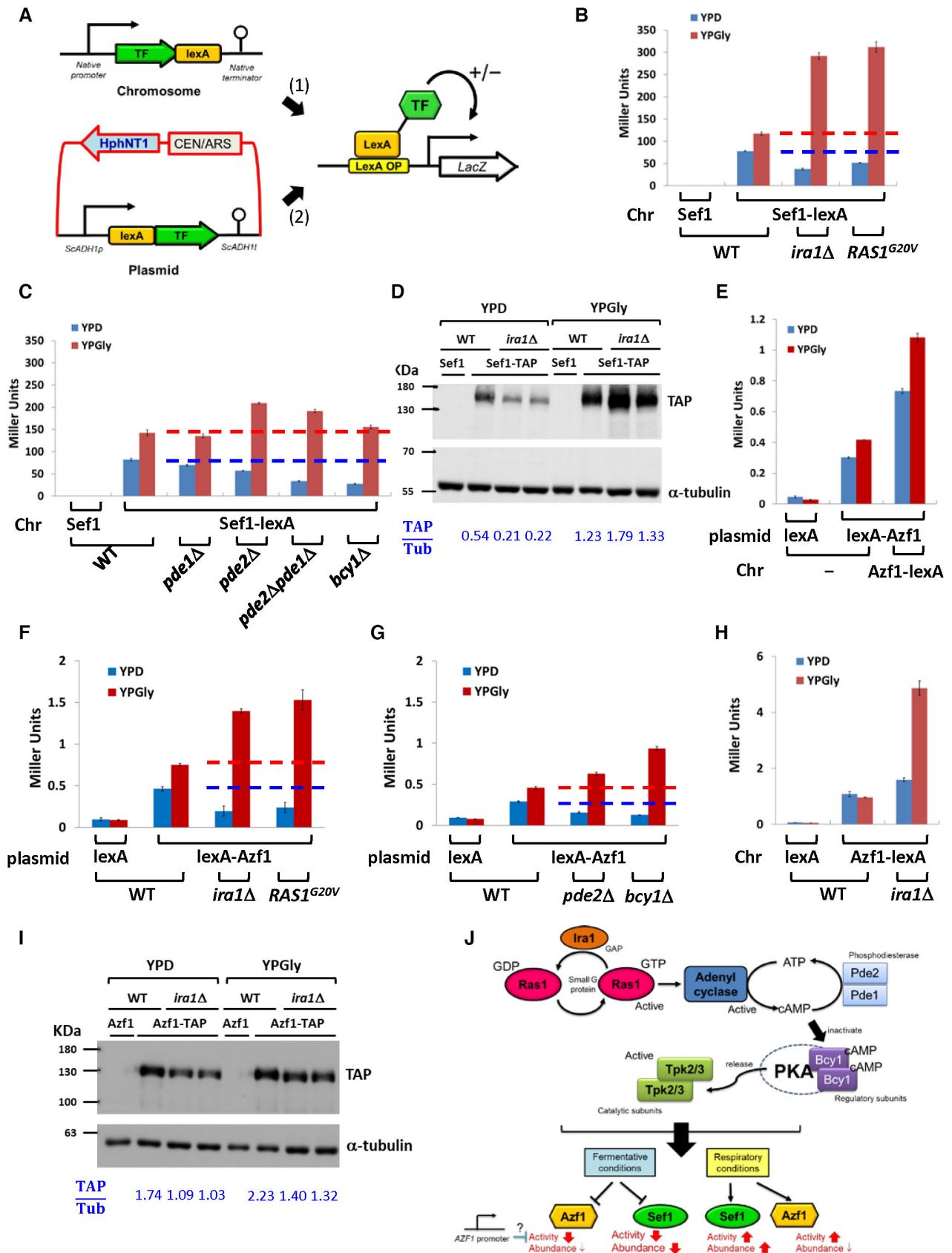
Figure 3.

that glycolysis in the *azf1Δ* cells may be particularly vulnerable. Indeed, both the *azf1Δ* and *sef1Δazf1Δ* mutant lines proved more sensitive to the glycolysis inhibitor, 2-deoxyglucose (Laussel & Léon, 2020), especially at higher temperatures (Fig 4B and C, and Appendix Fig S9A and B).

Moreover, we noticed that several major negative regulators of the Ras1-PKA pathway, including the aforementioned *IRA1* and *BCY1*, were downregulated under the YPD condition (Fig 4D). Considering that Ras1-PKA is also a glucose-responsive signaling pathway (Conrad *et al*, 2014), misexpression of those negative regulators may contribute to the "Dex-trade-off" effect due to conflict between the hyperactive Ras1-PKA pathway and the phenotypic impacts of other *azf1Δ*-driven gene misregulations (Fig 4E). To test that idea, we deleted *IRA1* and *AZF1* in the wild-type or *sef1Δ* background to mimic the extreme downregulation of *IRA1*. Interestingly, both the *azf1Δira1Δ* and *sef1Δira1Δazf1Δ* mutant lines showed a heat stress-induced synthetic growth defect under both YPD and YPGly conditions (Fig 4F and Appendix Fig S9C). Furthermore, the spores carrying both the mutated *ira1* and *azf1* alleles from tetrads of mating products between 28°C-Evo and 39°C-Evo suppressors also exhibited the synthetic growth defect (Appendix Fig S10A and B). These results not only support the notion that misregulation of the Ras1-PKA pathway participates in the "Dex-trade-off" effect of *azf1Δ* but also provide corroborating evidence that Ira1 and Azf1 belong to the same functional module.

Similarly, subsequent examination of downregulated genes relating to the GO term "alpha-amino acid metabolic process" implied that multiple genes involved in Ser, Cys, Asp, Lys, Met, Gln, Glu, Pro, Arg, and Ile metabolism may be defective (Appendix Fig S11A). This scenario is supported by the exacerbated delay in growth (longer lag-phase) of the *azf1Δ* and *sef1Δazf1Δ* mutants when cells were pre-starved in an amino acid-depleted medium (Appendix Fig S11B). Notably, we observed delayed growth at normal temperature, which was more severe under heat stress. Thus, taken together, our findings show that under the YPD condition, the *azf1Δ* mutation places cells in a state of poor core carbon and nitrogen metabolism so that their growth further deteriorates under heat stress, contributing to the "Dex-trade-off" effect.

Beneficial effects of the loss-of-function *azf1* mutation

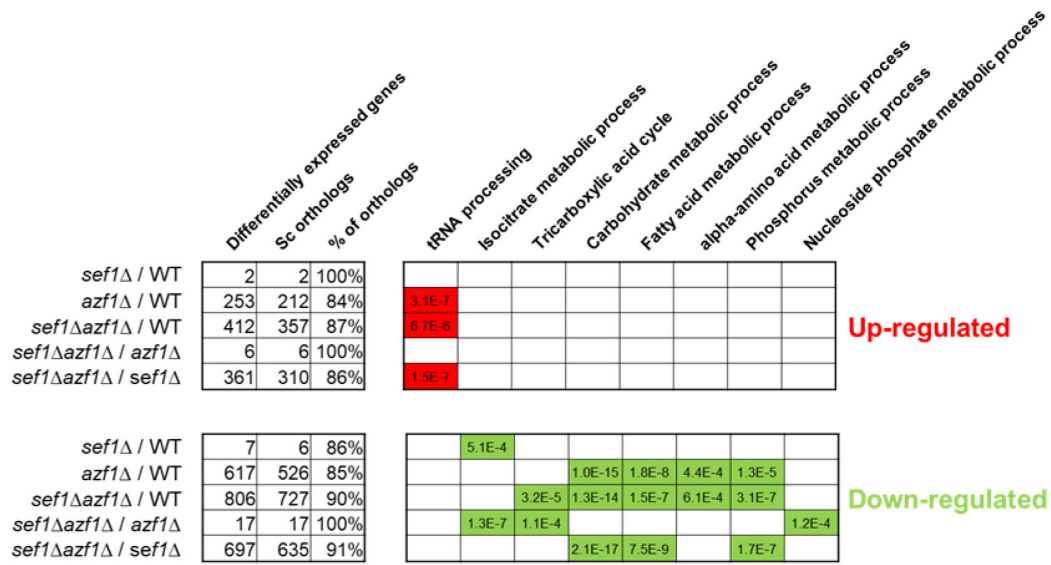To connect altered gene expression with the "Gly-compensation" effect, we investigated the enriched GO term list under the YPGly condition (Fig 5A). The *azf1Δ*-driven group displays a consistent pattern of enriched GO terms relating to upregulation of the cell cycle, cytoskeleton organization, DNA repair and replication, response to stress, vesicle-mediated transport, and chromatin silencing, as well as downregulation of genes related to ribosome/rRNA and tRNA metabolism that are key components in translation. In contrast, the *sef1Δ*-driven group only displays consistent enrichment for GO terms pertaining to downregulation of the TCA cycle, as reported in a previous study (Hsu *et al*, 2021).

The "response to stress" GO term enriched in the *azf1Δ*-driven group encompasses 186 upregulated genes, including core heat-shock response genes and especially heat-shock proteins (HSPs; Appendix Fig S12A, see "Heat" and "Protein folding" sub-GO groups), implying a possible link between upregulated HSPs and "Gly-compensation" under heat-stressed conditions. HSPs play pivotal roles in protein folding and refolding, as well as in responses to heat and other stresses, and they are globally induced by the transcriptional regulator Hsf1, which is conserved across species (Veri *et al*, 2018). As expected, we found that a hypomorphic (diminished function) *hsf1* mutation partially abrogated the upregulation of representative HSP genes in response to *azf1Δ* (Appendix Fig S12B), thereby partially limiting the "Gly-compensation" effect in both *azf1Δ* and *sef1Δazf1Δ* mutant lines (Fig 5B). That outcome indicates that the higher basal levels of HSPs induced by Hsf1 contribute to *azf1Δ*-induced heat resistance. Moreover, we identified a total of 212 genes related to ribosome/rRNA metabolism and a further 75 genes related to tRNA metabolism that were downregulated in response to *azf1Δ* (Appendix Fig S13), demonstrating a typical yeast environmental stress response (ESR) in gene expression that involves coupling the upregulation of stress defense genes with downregulation of ribosome biogenesis/protein synthesis genes (Gasch *et al*, 2000; Ho & Gasch, 2015; Taymaz-Nikerel *et al*, 2016).

Furthermore, we noted that the TCA cycle GO term is not enriched among the downregulated genes of the *azf1Δ*-driven group, especially for *sef1Δazf1Δ*/wild-type, unlike the *sef1Δ*-driven group (Fig 5A). Indeed, deletion of *AZF1* not only partially restored expression of TCA cycle genes under the YPGly condition (Fig 5C) but it also rescued cellular respiration [as assayed by triphenyl tetrazolium chloride (TTC) reduction assay] (Appendix Fig S14A), thus reinforcing the "Gly-compensation" effect.

Apart from glycerol, both ethanol and acetate are common non-fermentable carbon sources preferred by yeast species during respiratory growth, and that trigger a series of coordinated gene

A

	Differentially expressed genes	Sc orthologs	% of orthologs	tRNA processing	Isocitrate metabolic process	Tricarboxylic acid cycle	Carbohydrate metabolic process	Fatty acid metabolic process	alpha-amino acid metabolic process	Phosphorus metabolic process	Nucleoside phosphate metabolic process	
sef1Δ / WT	2	2	100%									
azf1Δ / WT	253	212	84%	3.1E-7								**Up-regulated**
sef1Δazf1Δ / WT	412	357	87%	6.7E-6								
sef1Δazf1Δ / azf1Δ	6	6	100%									
sef1Δazf1Δ / sef1Δ	361	310	86%	1.5E-7								

sef1Δ / WT	7	6	86%	5.1E-4								
azf1Δ / WT	617	526	85%				1.0E-15	1.8E-8	4.4E-4	1.3E-5		**Down-regulated**
sef1Δazf1Δ / WT	806	727	90%			3.2E-5	1.3E-14	1.5E-7	6.1E-4	3.1E-7		
sef1Δazf1Δ / azf1Δ	17	17	100%	1.3E-7	1.1E-4						1.2E-4	
sef1Δazf1Δ / sef1Δ	697	635	91%				2.1E-17	7.5E-9		1.7E-7		

B 28°C   **C** 37°C

D

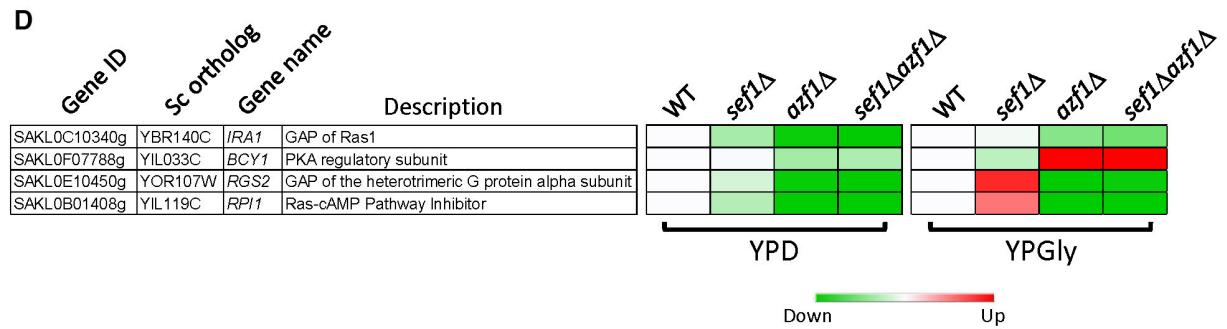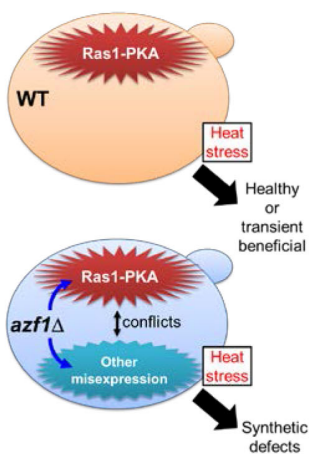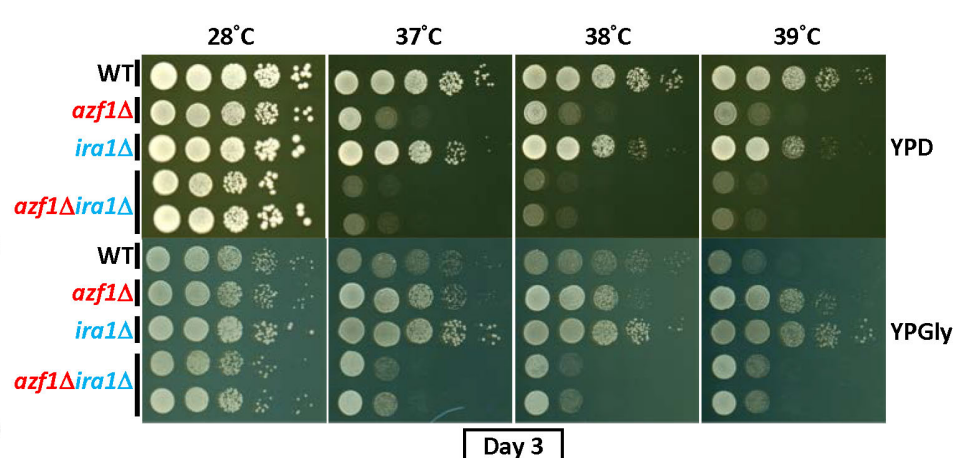| Gene ID	Sc ortholog	Gene name	Description
SAKL0C10340g	YBR140C	IRA1	GAP of Ras1
SAKL0F07788g	YIL033C	BCY1	PKA regulatory subunit
SAKL0E10450g	YOR107W	RGS2	GAP of the heterotrimeric G protein alpha subunit
SAKL0B01408g	YIL119C	RPI1	Ras-cAMP Pathway Inhibitor

E   **F**

Figure 4.

◀

Figure 4. Phenotypic response to *azf1Δ* mutation in the YPD condition.

A Selected GO terms enriched under the YPD condition. The adjusted *P*-values of the hypergeometric test with Bonferroni correction are shown.
B, C Hypersensitivity of *azf1Δ* mutants to 2-deoxyglucose under the YPD condition without heat stress (28°C) (B) or with mild heat stress (37°C) (C).
D The major negative regulators of the Ras1-PKA pathway are downregulated in response to *azf1Δ* mutation under the YPD condition. The heatmap was generated from the mean TPM (Transcripts Per Million) ratio of RNA-seq data relative to wild-type for each condition. The high-resolution source table of the heatmap is provided in Dataset EV17.
E A proposed model describing how a hyperactive Ras1-PKA pathway due to downregulation of negative regulators (in the *azf1Δ* mutant) or *ira1Δ* mutation (used in experiments) is incompatible with the other gene misexpression induced by *azf1Δ*.
F The synthetic growth defect of *azf1Δira1Δ* under the wild-type background in heat-stressed conditions.

expression patterns (Turcotte *et al*, 2009). Interestingly, in contrast to the pronounced beneficial impact of glycerol, we found that acetate only provided a weak heat stress-specific benefit to the *azf1Δ* strains, whereas ethanol did not appear to exert any benefit (Appendix Fig S14B). The same defective growth was observed in the post-diauxic growth phase of the *azf1Δ* mutant grown in YPD when ethanol was the major carbon source (Appendix Fig S11B). To link this glycerol-specific trait to gene expression, we examined more closely the YPGly-based RNA profiles of the core non-fermentable carbon metabolic pathways of glycerol utilization (uptake and breakdown), pyruvate production, and pyruvate utilization (more specifically, the PDH-dependent respiratory pathway and the PDC-dependent fermentative pathway; Fig 5D). We present in Appendix Fig S14C the remodeled glycerol usage pathways and the predicted metabolic flux in *azf1Δ* cells (relative to wild-type) according to the differential gene expression summarized in Fig 5D. In Appendix Fig S14D, we propose a model of glycerol-driven metabolic remodeling according to Appendix Fig S14C. Our model is based on the notion that *azf1Δ* cells maintain a high intracellular concentration of glycerol and its derivatives due to increased uptake and restricted pyruvate production (from DHAP to pyruvate), with biased pyruvate flux fueling the TCA cycle due to strong competition for pyruvate between high-affinity mitochondrial pyruvate carriers plus the PDH complex and the low-affinity PDC complex (Pronk *et al*, 1996; Møller *et al*, 2004).

Moreover, according to the classical definition of "compensation," a compensatory mutation is a modifier (second) mutation that masks or completely suppresses the defects from the major (first) mutation, and this amelioration should show greater phenotypic gains in the genotypes with the major mutation than the one without (Moore *et al*, 2000; van Leeuwen *et al*, 2016). That is, there should be positive epistasis between a compensatory mutation (e.g., loss-of-function *azf1*) and the major mutation (e.g., *sef1Δ*). To test this idea, we examined the *azf1Δ*-induced compensation in gene expression between the *sef1Δ* and wild-type backgrounds. As expected, the majority of TCA cycles genes were higher upregulated by *azf1Δ* under the *sef1Δ* than the wild-type background (Fig EV3A), indicating a clear positive epistasis between *azf1Δ* and *sef1Δ* genotypes (Fig EV3B). Similar positive-magnitude epistasis in the differential expression of glycerol utilization and auxiliary pathways as well as the stress-responsive genes are shown in Fig EV3C–E. Taken together, these results clearly demonstrated that the beneficial *azf1Δ* causes *sef1Δ*-specific compensation in gene expression.

Hence, the loss-of-function *azf1* mutation induces "Gly-compensation" by: (i) increasing basal transcriptional levels of stress-defense genes; (ii) restoring TCA cycle gene expression; and (iii) transcriptionally remodeling the metabolic pathways to favor glycerol utilization and more efficient respiration.

azf1Δ cells display cell density-dependent "Dex-trade-off" traits and an evolutionary counteracting strategy

Intriguingly, during growth assays, we noticed unexpectedly that the "Dex-trade-off effect" in *azf1Δ* cells could be alleviated by gradually increasing the initial cell density (Appendix Fig S15). More specifically, the maximal growth rate of *azf1Δ* cells under "Dex-trade-off" conditions was restored to a near wild-type level when growth was initiated at a higher inoculum size (Fig 6A), hinting that a cell density-dependent mechanism plays a role in combatting the "Dex-trade-off effect." To prevent extinction, *S. cerevisiae* cells may display cell density-dependent cooperative behavior to enable each other and their future generations to survive and replicate at high temperatures (Laman Trip & Youk, 2020). To address if *L. kluyveri* cells can cooperatively help *azf1Δ* cells survive, we grew Azf1-sufficient (denoted *AZF1*) and *azf1Δ* strains independently in separate cultures or co-cultured together and measured the fitness of *azf1Δ* cells relative to the *AZF1* strain by counting viable cell numbers after 20 h of growth under the "Dex-trade-off" condition (Appendix Fig S16A). Growth curves (Appendix Fig S16B) revealed that the relative fitness of *azf1Δ* cells increased under co-culture conditions relative to the independent culture in both wild-type and *sef1Δ* backgrounds (Fig 6B and C). Similar cooperative growth assays on an agar surface (Appendix Fig S16C) generated results consistent with those from the equivalent aforementioned experiments in media (Appendix Fig S16D and E). Taken together, these results indicate enhanced survival of *azf1Δ* cells under "Dex-trade-off" conditions can be facilitated by the presence of surrounding *AZF1* cells, mimicking the scenario by which low-frequency trade-off mutants can be maintained in a heterogeneous population.

One mechanism by which cell density-dependent cooperative behavior operates in yeast is secretion of glutathione into the extracellular environment (Laman Trip & Youk, 2020). The level of glutathione secretion required for growth under heat-stressed conditions depends on the cell population density before extinction. Although it remains unclear how extracellular glutathione helps cells to survive, one study has shown that a mild concentration of surfactants (such as sodium dodecyl sulfate, SDS) to increase cell permeability increased the extracellular concentration of glutathione (Wei *et al*, 2003). Other studies have indicated that glutathione is required for bacterial and yeast responses to osmotic stress (Smirnova *et al*, 2001; Jamnik *et al*, 2006) and that it serves as an osmotic driving force in bile formation (Jamnik *et al*, 2006). Taken together, these findings prompt the hypothesis that cell density-dependent cooperative behavior under heat stress may be linked to an osmotic imbalance of cells. Moreover, glutathione might be one but not the only factor contributing to this survival strategy.
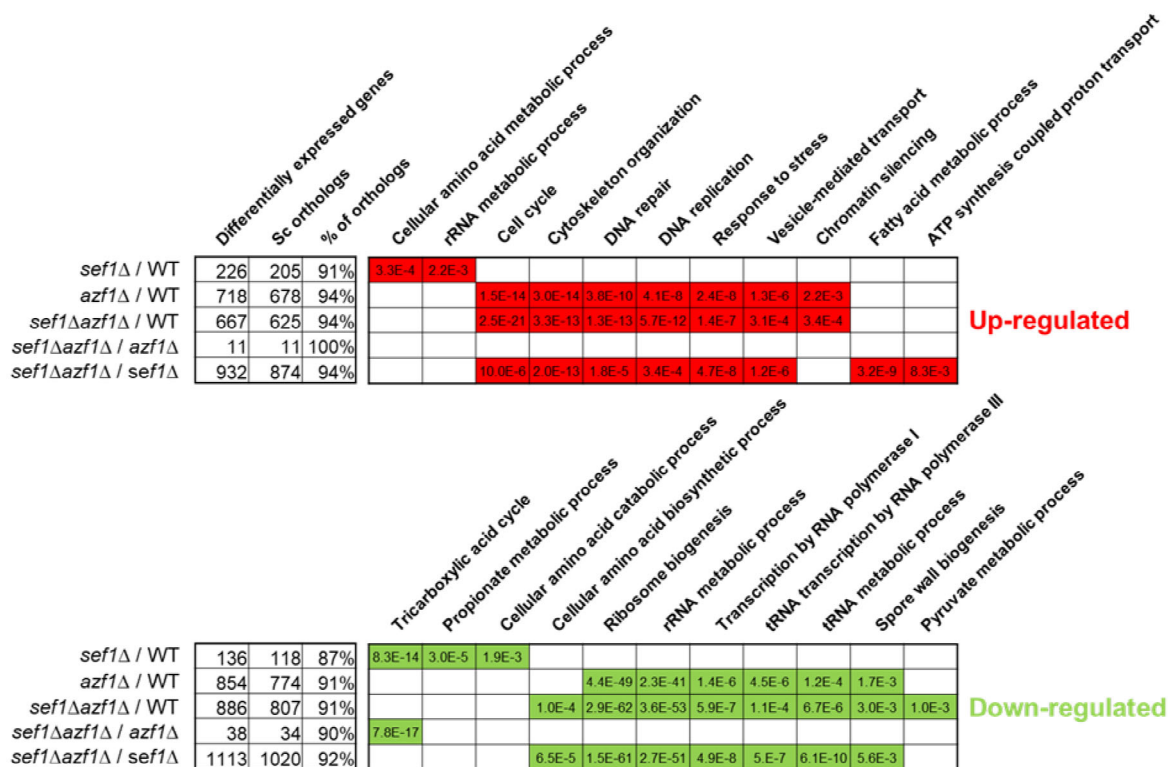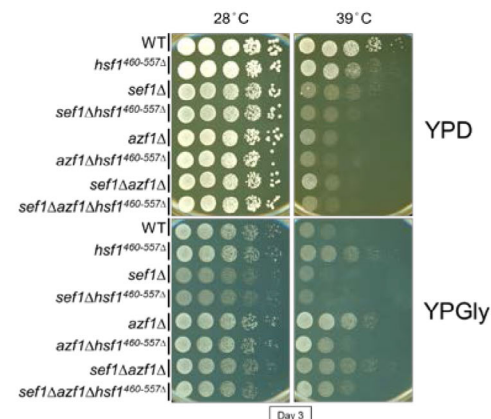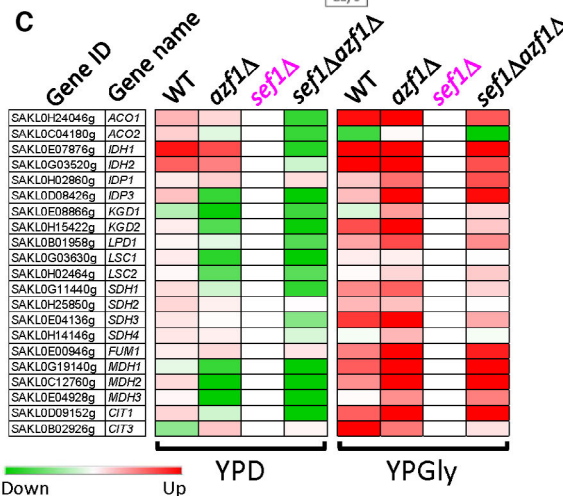
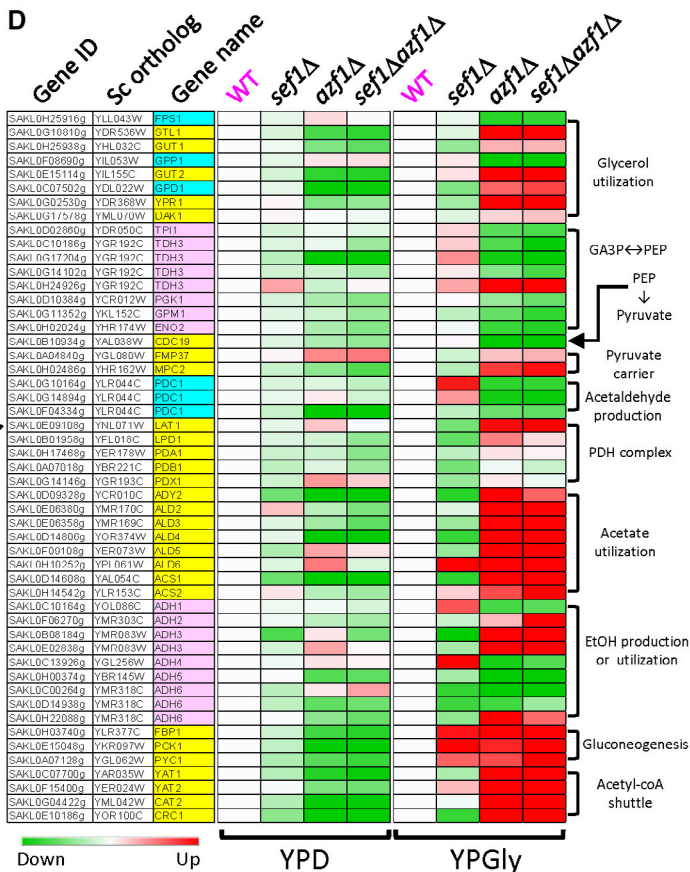**Figure 5.**

◄

Figure 5. Phenotypic response to *azf1Δ* mutation in the YPGly condition.

A   Selected GO terms enriched under the YPGly condition. The adjusted *P*-values of the hypergeometric test with Bonferroni correction are shown.
B   The counteracting effect of hypomorphic *hsf1* on growth in response to *azf1Δ* mutation in both wild-type and *sef1Δ* backgrounds. *HSF1* is an essential gene in yeast (Solís Eric *et al*, 2016), so a hypomorphic *hsf1* mutation with a truncated C-terminus (460–557 amino acids removed; Sorger, 1990) rather than a null mutant was used in *L. kluyveri* strains.
C   Partial compensation of defective TCA cycle gene expression in *sef1Δ* mutants by *azf1Δ* mutation under the YPGly condition. The heatmap was generated using the mean TPM ratio from RNA-seq data relative to the *sef1Δ* strain under each condition.
D   Transcriptional remodeling of the core glycerol utilization and auxiliary pathways in response to *azf1Δ* mutation under the YPGly condition. The heatmap was generated using the mean TPM ratio from RNA-seq data relative to the wild-type under each condition. The high-resolution source tables of the heatmaps are provided in Dataset EV17.

Accordingly, we wondered if *azf1Δ* cells displaying cell density-dependent cooperative behavior also present an osmotic imbalance. Despite our gene expression data indicating that *azf1Δ* cells do not preferentially utilize ethanol, that finding is still insufficient to explain the ineffectiveness of ethanol (unlike glycerol) against heat stress. Consequently, we explored if ethanol is also a stressor of cells (Stanley *et al*, 2010), especially when cell wall integrity (CWI) is compromised (Udom *et al*, 2019). As expected, compared to wild-type, all *azf1Δ* cells not only displayed higher permeability to the dye phloxine B (Fig 6D), but they were also more sensitive to mild cell wall disruption elicited by zymolyase treatment, especially when cells were pre-grown under heat-stressed conditions (Fig 6E). Moreover, our finding that gene expression of a vital cell wall glyco-protein (*CIS3*) and twoβ-1,3-glucanosyltransferases (*GAS1* and *GAS5*) required for CWI in yeast (Tomishige *et al*, 2003; Mazáň *et al*, 2008) are all downregulated in *azf1Δ* cells (Fig 6F) supports the notion that the *azf1Δ* mutants have a weakened CWI. Intuitively, a weakened cell wall (or outer membrane) will trigger hypo-osmotic stress in cells, leading to cell bursting if the condition is aggravated. Osmotic rebalancing by supplementing the medium with sorbitol can suppress growth defects caused by cell bursting (Lee *et al*, 1993; Serrano *et al*, 2006; Beese *et al*, 2009). We observed complete osmotic rebalancing in *azf1Δ* mutant cells upon adding 1.5 M of sorbitol into YPD (Fig 6G), implying that the defective CWI of *azf1Δ* cells alters their optimal osmolarity required for growth and also contributes to their "Dex-trade-off" phenotypes. Interestingly, we detected no clear differential gene expression related to glutathione in response to the *azf1Δ* mutation, indicating that further work is needed to identify the distinct mechanism by which Azf1 in *L. kluyveri* regulates this cell density-dependent cooperative behavior.

Discussion

Perturbing the Azf1 transcriptional network can rapidly compensate for disruption of the Sef1 transcriptional network

Our rapid suppressor development strategy allowed us to initiate an evolutionary repair experiment to determine responses to the *sef1Δ* mutation and to generate a large number of evolved lines carrying early and strongly beneficial mutations with the potential to compensate for the *sef1Δ*-caused defects. By performing selection on agar plates, clonal interference (Gerrish & Lenski, 1998) among cells carrying beneficial mutations could be minimized, thereby circumventing a pervasive issue when evolving asexually reproducing

organisms in liquid broth (Barrick & Lenski, 2013; Van den Bergh *et al*, 2018; McDonald, 2019) and maintaining the early adaptive diversity of beneficial mutations (Levy *et al*, 2015; Blundell *et al*, 2019). Surprisingly, after phenotyping 240 suppressor clones from two independent lineages, we found that the majority (87.5%) displayed a consistent phenotypic pattern across all tested conditions. Subsequent sequencing and verifications by genetic and phenotypic analyses suggested that they carried a higher proportion of causal mutations hitting *IRA1* or *AZF1* and other unidentified genes related to Ira1 or Azf1 functions (Figs EV1 and EV2). That finding demonstrates clear evolutionary parallelism and unexpectedly restricted diversity arising from *sef1Δ*-adaptive mutations in this batch of the suppressor development experiment.

We consider three possible reasons for that outcome. First, our suppressor colony-picking strategy could have been biased because we picked the biggest colonies on the agar plates (Appendix Fig S2) and clones of similar fitness most likely carry similar causal mutations, as described above for the beneficial *ira1Δ* mutation. Second, pre-existing low-frequency beneficial mutations in the founder colony may have been selected, with this latter scenario being supported by our identification of the presence of identical mutation types in separate suppressor clones. Indeed, we identified many such cases (Figs 2C and D, and EV1B and EV2B). Identical mutations are less likely to form independently by chance in an asexual population, so we conclude that these mutations, at least in this batch of the experiment, may have pre-existed in the quasi-species founder colony that was picked (Appendix Fig S1D and E), acting as rapid adaptive solutions to the changing environment (Teng *et al*, 2013). Third, the specific type of driving forces may induce specific mutations, as supported by the triple beneficial effects of "restored respiration" (Fig 5C and Appendix Fig S14A), "elevated heat-shock defense" (Appendix Fig S12), and "augmented glycerol utilization" (Fig 5D) elicited by the *azf1* mutation, which together are required for cell survival under our heat-stressed YPGly condition.

Notably, the *azf1* mutations also partially restored the defective TCA cycle gene expression in *sef1Δ* mutants under the YPGly condition (Fig 5C). This suggests that massive transcriptomic perturbations accompanying fitness restoration might be a general mechanism to facilitate compensatory evolution, as revealed by other studies (Szamecz *et al*, 2014; McCloskey *et al*, 2018). However, how *azf1* loss-of-function assists to stabilize a new transcriptional network without Sef1 is still unclear. We conducted a simple experiment to test whether Azf1 affects *IDH2* expression directly or indirectly in *L. kluyveri*. The *IDH2* is a TCA cycle gene directly regulated by Sef1 (Hsu *et al*, 2021), and its promoter carries one
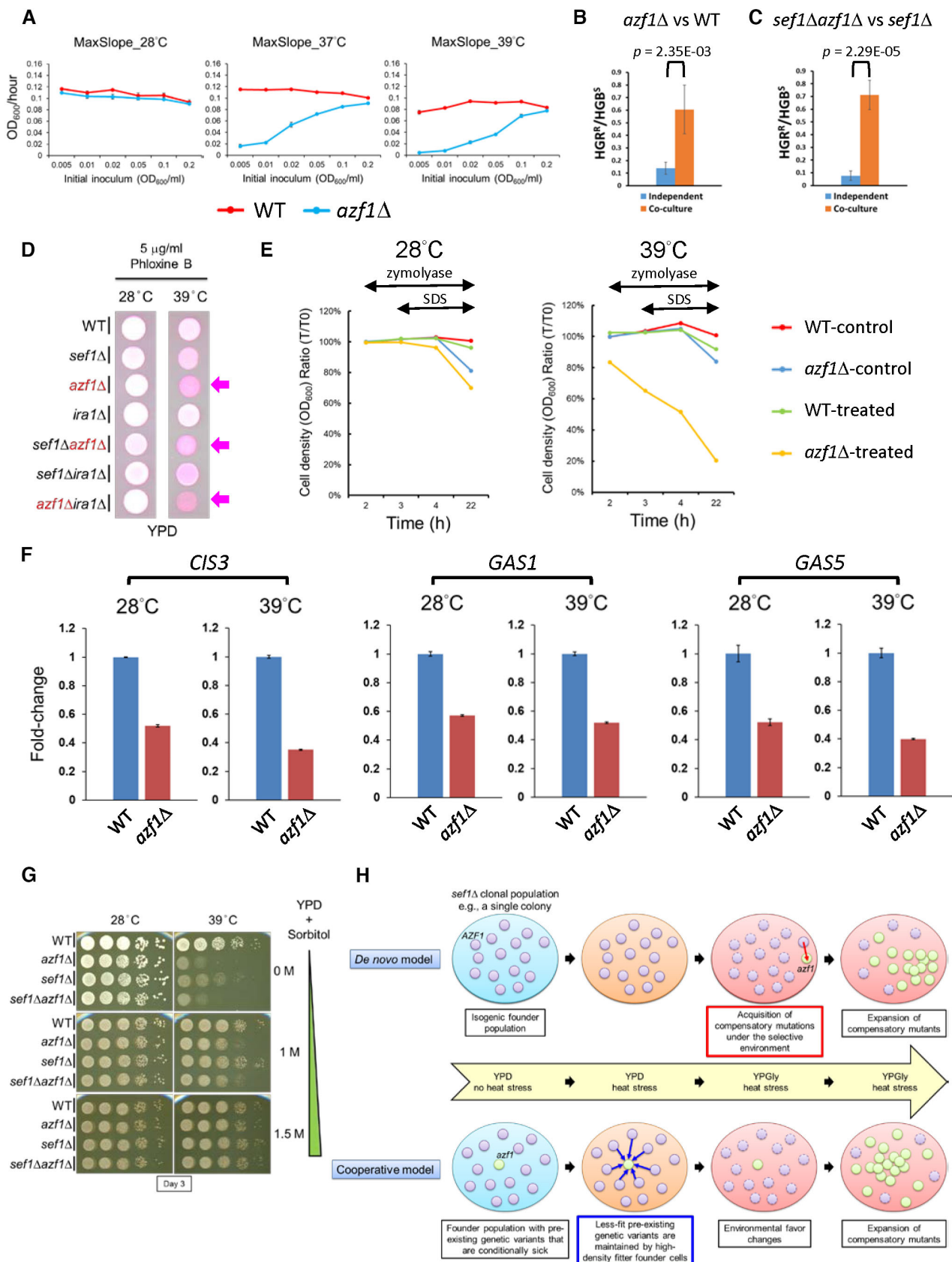
Figure 6.

◀

Figure 6. The trade-off phenotype of *azf1Δ* mutants is linked to cell wall integrity.

A The effect of inoculum density on the mean maximal growth rate of the *azf1Δ* population in YPD under heat-stressed conditions. The growth curves were measured by using a Tecan plate reader with intermittent shaking. Results are displayed as average max slopes ± SD from three technical repeats.

B, C (B) The *azf1Δ* cells are more persistent when co-grown with wild-type cells in liquid broth under the "Dex-trade-off" condition. (C) The *sef1Δazf1Δ* cells are more persistent when co-grown with *sef1Δ* cells in liquid broth under the "Dex-trade-off" condition. For (B) and (C), results are displayed as average HGB^R/HGB^S ± SD from six technical repeats. HGB^R/HGB^S represents the ratio of HGB-resistant and HGB-sensitive colony numbers. Statistical significance tests were carried out using unpaired Student's *t*-tests.

D Under the "Dex-trade-off" condition, *azf1Δ* cells were more severely stained by Phloxine B (pink color). Phloxine B is a negatively charged dye that only stains cells intracellularly when cell membrane intactness has been compromised (Grosfeld *et al*, 2021). The arrows indicate the *azf1Δ*-containing cells that stain heavily by Phloxine B.

E The *azf1Δ* mutant is more sensitive to mild cell wall disruption. The cells pre-grown at indicated temperatures in YPD were first treated with 60 units/ml zymolyase at room temperature for 2 h, and then 0.1% SDS was added into the suspension to facilitate cell lysis. Cell intactness (*y*-axis) was calculated as the ratio of cell density (OD$_{600}$/ml) at specific time points relative to T$_0$. Untreated samples were used as the control.

F Expression of *CIS3* (SAKL0C05676g), *GAS1* (SAKL0H00550g), and *GAS5* (SAKL0F05456g) in response to *azf1Δ* mutation under the YPD condition. The relative fold change of each gene is shown as $2^{-\Delta\Delta C_T}$, using *CDC34* (SAKL0D02530g) as the endogenous control and the ΔC_T value from the wild-type sample as the corresponding calibration value. Expression levels are displayed as mean fold-changes ± SD from three technical repeats.

G The addition of sorbitol to the YPD medium to enhance osmolarity suppressed the "Dex-trade-off" phenotype of the *azf1Δ* mutants.

H *De novo* and cooperative models can explain the rapid evolutionary repair of *sef1Δ* mutation-induced phenotypes by *AZF1* loss of function. In the *de novo* model, the *azf1* mutant newly forms under the selection brought about by *sef1Δ*-suppressive mutations. In the cooperative model, the *azf1* mutant pre-exists as a quasi-species in the founder population, its persistence being cooperatively supported by its fitter neighboring founder cells under the trade-off conditions, but it is then selected and undergoes population expansion to be dominant under favorable environmental conditions.

confirmed Sef1-binding motif and one putative Azf1-binding motif adjacent to each other (Appendix Fig S17A and B). We deleted the putative Azf1 motif on the *IDH2* promoter in the wild-type and found out this motif loss did not lead to the upregulation of *IDH2* the same as *azf1Δ* did (Appendix Fig S17C). This finding suggests that *azf1Δ* upregulates TCA cycle genes indirectly, possibly through other down-regulated transcriptional regulators in response to *azf1Δ* (Dataset EV15), especially through those transcriptional repressors (Appendix Fig S17D). Elucidating the contributions of these factors to the *azf1Δ*-induced gene expression is a potential direction in the future.

The *sef1Δ* does not provide a strong founder effect to the evolutionary trajectories

Given the potential for founder effects and epistasis (Barrick *et al*, 2010; Jerison *et al*, 2017; Wünsche *et al*, 2017; Rojas Echenique *et al*, 2019), we wondered whether the *sef1Δ* founder genotype constrained or shaped the evolution trajectories. We first confirmed that *sef1Δ* did not result in higher suppression rates than the wild-type did in our suppressor-developing conditions by using fluctuation assays (see "mutation rates" in Appendix Fig S18A and B). Then, we demonstrated that *ira1Δ* and *azf1Δ* did not cause better fitness improvement (positive epistasis) in the *sef1Δ* than in the wild-type backgrounds by using epistasis analyses (Dataset EV13). These two results not only suggest that there is no strong founder effect of *sef1Δ* but also imply that the wild-type cells could also evolve in this way. Therefore, we performed a new batch of suppressor development at 28 and 39°C including the wild-type (Dataset EV16). In the 28°C-WT-Evo clones, although at a lower frequency (3 of 20), we still identified evolved clones showing desiccation hypersensitivity (suggesting the occurrence of *ira1* loss-of-function mutations or other mutations in related pathways; Fig EV4A). Similarly, in the 39°C-WT-Evo clones, we also identified 5 of 20 evolved clones showing "Dex-trade-offs" (suggesting the occurrence of *azf1* loss-of-function mutations or other mutations in related pathways). Notably, the new batch MATa and MATα 28°C-

sef1Δ-Evo clones still showed a high frequency of desiccation hypersensitivity (18/19 and 17/20, respectively) similar to the first batch (Fig EV4A). In contrast, the new batch MATa and MATα 39°C-*sef1Δ*-Evo clones did not have a high frequency of "Dex-trade-off" suppressors (2/20 and 3/20, respectively; Fig EV4B). We think the picked quasi-species founder colonies might still contribute to this discrepancy between two batches of suppressor development experiments.

Nevertheless, our findings raise a hypothesis that the *ira1* and *azf1* mutants can form subpopulations in the wild-type population first and then alleviate the deleterious effects of the following spontaneous *sef1* mutations (Fig EV5). This strategy may allow the *sef1* mutations to be fixed in the population as long as the *sef1* mutants are not less competitive in future environments.

Glucose, Ras1-PKA signaling, and Azf1

The beneficial effects of the *ira1* loss-of-function mutation arise from hyperactive Ras-PKA signaling, leading to uncontrolled cell growth in the absence of the yeast growth-promoting factor glucose, reminiscent of tumor cell growth (Cazzanelli *et al*, 2018). That mutation exerted a more general fitness-improving impact (at least in the conditions used in our study), eliciting a "double-compensation" effect irrespective of the YPD and YPGly conditions. In contrast, the *azf1* loss-of-function mutation is pleiotropic in terms of the aforementioned triple beneficial effects and its deleterious impacts relating to mildly defective core carbohydrate metabolism (Fig 4 and Appendix Fig S8), amino acid metabolism (Appendix Fig S11), and CWI (Fig 6). All those defects only arose under the YPD condition and they were exacerbated by heat stress, indicating that they represent life-history "trade-offs" (Garland, 2014) and that the *azf1* mutant cells are typical specialists (Van den Bergh *et al*, 2018).

Interestingly, although Azf1 appears functional under both glucose and glycerol conditions, we believe that glucose is the environmental factor sensed by Azf1, that is, Azf1 regulates gene expression in response to the presence or absence of glucose. This speculation is supported by the facts that: (i) Azf1 activity is

regulated by the Ras1-PKA pathway (Fig 3), which is mainly glucose responsive in yeast (Conrad *et al*, 2014; Cazzanelli *et al*, 2018); (ii) *azf1Δ* triggered the opposite expression pattern between stress response and ribosomal genes (Appendix Figs S12A and S13). This opposite expression pattern is also regulated by the PKA pathway in response to the glucose availability (Conrad *et al*, 2014); and (iii) the presence of glycerol in YPD did not convert "Dex-trade-off" to "Gly-compensation" (Appendix Fig S19), implying that glucose is the trigger. Elucidating the molecular components involved in these processes is an interesting topic for future exploration.

Cooperation maintains trade-off genotypes

We have revealed that pleiotropic defects (misregulation of multiple TCA genes due to the *sef1Δ* mutation in this study) can be simultaneously compensated in a short timeframe simply by means of another pleiotropic change (i.e., *AZF1* loss of function). Despite potentially being maintained by balancing selection (Mérot *et al*, 2020), this new pleiotropic change may remain concealed by accompanying trade-offs within a short evolutionary timescale, especially in unstable environments (Chen & Zhang, 2020). Here, we have demonstrated cell density-dependent mitigation of such trade-offs, whereby *azf1Δ* individuals can persist when densely surrounded by founder cells or until the density of *azf1Δ* progeny exceeds a threshold (Fig 6A–C and Appendix Fig S16D and E). Although the underlying mechanism remains unknown, this "cooperative persistence" enhances the adaptive potential not only of *de novo azf1* mutants when unfavorable environments are encountered but also of pre-existing *azf1* mutants before experiencing selection (Fig 6H), enabling a contingent secondary adaptive step to repair the trade-offs (Aggeli *et al*, 2021).

Frequency-dependent selection (FDS) describes how the fitness of a genotype or phenotype in a population is related to its frequency in the population (Ayala & Campbell, 1974). Positive FDS is a selection regime whereby the fitness of a phenotype increases with its frequency (Ayala & Campbell, 1974). The cell density-dependent mitigation of trade-offs in *azf1Δ* cells represents a simple case of positive FDS. In early models, positive FDS was predicted to reduce diversity due to systematic loss of rare polymorphisms. However, more recent theories predict that positive FDS maintains rather than reduces diversity when populations patchily occupy spatially structured habitats (Molofsky *et al*, 2001; Molofsky & Bever, 2002; Rendueles *et al*, 2015). Our evolutionary repair experiments, with characteristics of changing environments (fermentative vs. respiratory; normal vs. heat stressed), local habitats (growth on agar plates), and cell density-dependent cooperation, is an intuitive example showing that positive FDS maintains microbial diversity and facilitates evolution.

The *sef1Δ*-suppressive mutations of *AZF1* compensate for perturbed expression of vital TCA cycle genes under selective conditions, reflecting a type of evolutionary tinkering and stabilizing selection (Lavoie *et al*, 2010; Signor & Nuzhdin, 2018, 2019). The multiple beneficial and trade-off mutations that accumulate as a consequence of ongoing evolutionary repair processes represent a good source of molecular diversity (LaBar *et al*, 2020). From the perspective of the macroevolution of transcriptional networks, our study illuminates how compensatory evolution facilitates the stabilization of TCA gene expression under specific conditions. The compensatory evolution maintains the fitness of the mutant cells losing Sef1 and allows a new transcriptional regulatory network without Sef1 to persist, enabling transcriptional rewiring to continue.

Materials and Methods

Genome resources

The genome sequence of *Lachancea kluyveri* (CBS 3082) was originally from Bioproject accession number PRJNA1445. The sequence and improved annotation can be downloaded from the GRYC (Genome Resources for Yeast Chromosomes; http://gryc.inra.fr) database (Brion *et al*, 2015; Hsu *et al*, 2021). The sequences and structures of the *L. kluyveri* MATa and MATα loci were as per contigs under accession numbers AACE03000005 (Consortium *et al*, 2009) and AACE01000014 (Butler *et al*, 2004), respectively.

Strains and plasmid construction

To avoid confusion, we have adopted the term "wild-type" to describe the parental genotypes used in our study, each of which may carry auxotrophic mutations or specific genetic manipulations, and they acted as reference strains for all comparative experiments unless otherwise stated. The *L. kluyveri* strains, primers, and plasmids used in this study are listed in Dataset EV14. All DNA fragments used in cloning were PCR amplified using Phusion High-Fidelity DNA polymerase (F530L, Thermo Fisher Scientific, USA). The PCR products and restriction-digested products were purified by PCR cleanup or gel extraction using an AccuPrep® PCR/Gel Purification Kit (K-3037, Bioneer, Korea). DNA cloning into plasmids was achieved by using ligation (T4 DNA ligase, M180A, Promega, USA) or by means of an In-Fusion® HD Cloning Kit (639650, ClonTech by Takara, Japan). All plasmids were extracted and purified using a Presto™ Mini Plasmid Kit (PDH300, Geneaid, Taiwan). Successful strain constructions were confirmed by genomic DNA extraction, as described previously (Hsu *et al*, 2011), followed by PCR diagnostics using a homemade Taq DNA polymerase for genotyping.

For gene deletions, the DNA fragments of each deletion module consisting of a selection marker flanked by 5′ and 3′ sequences homologous to the target locus were created by overlap-extension PCR (Shevchuk *et al*, 2004). The genes deleted in this study are as follows: *SEF1* (SAKL0F12342g), *CHS3* (SAKL0C11726g), *AZF1* (SAKL0E10714g), *IRA1* (SAKL0C10340g), *PDE1* (SAKL0F00638g), *PDE2* (SAKL0D14344g), and *BCY1* (SAKL0F07788g).

For lexA and TAP tagging of Azf1, we used a modified (Hsu *et al*, 2021) SAT1 flipper method (Reuß *et al*, 2004). The TAP-tagging vector pSFS2A-TAPSacISacIIMut-28 has a second SacII site near the C-terminus of the TAP sequence, rendering cloning at the 3′ multiple cloning sites (MCS) problematic. To create a new TAP-tagging vector, we mutated the second SacII site by amplifying it from pSFS2A-TAPSacISacIIMut-28 using the primer pair TAP-1-ApaI and TAP-2-SacIIMut-XhoI, and then ligating the product between ApaI-XhoI sites in the pSFS2A vector to generate pSFS2A-TAP-New-2. The 978-bp C-terminal sequence (+1,480 to +2,457 of the ORF without the STOP codon) of *AZF1* was cloned into the pSFS2A-lexA-5 or pSFS2A-TAP-New-2 vectors between the KpnI-ApaI sites using

In-Fusion®, and the 411-bp 3'-UTR (terminator, +1 to +411 from the STOP codon) sequence of *AZF1* was ligated between the SacII-SacI sites to generate the lexA- or TAP-tagging plasmid for *AZF1*. The KpnI-SacI-digested fragments from both tagging plasmids were used to transform cells. The SklexAOPlacZ-1 reporter strain and derivatives were transformed to create chromosome-integrated Azf1 one-hybrid strains, whereas the JYL1897 wild-type strain and derivatives were transformed to generate Azf1-TAP strains. To produce plasmid-based Azf1 one-hybrid strains, the entire 2,460-bp *AZF1* ORF with STOP codon was cloned in-frame into pRS41H-lexA-3 between the BamHI-NotI sites downstream of the lexA sequence, thereby generating pRS41H-lexA-SkAzf1-1, and the plasmid was transformed into the SklexAOPlacZ-1 strain and derivatives. For Sef1, previously described one-hybrid and TAP-tagged strains were used (Hsu *et al*, 2021).

To create the *RAS1^{G20V}* hyperactive one-hybrid strains, we used the SAT1 flipper method. Gly20 of *RAS1* (SAKL0E10252g) was first mutated to Val by overlap-extension PCR-based site-specific mutagenesis (Sambrook, 2001). The 1,395-bp 5'-flanking region of the *RAS1^{G20V}* fragment (−424 from ATG to STOP) and its 297-bp 3' flanking region (+89 to +385 from STOP codon) were then ligated into the 5' and 3' MCSs of the pSFS2A vector between the ApaI-XhoI sites and the SacII-SacI sites, respectively. To transform cells, the ApaI-SacI-digested fragments from the pSFS2A-Ras1G20V-14 plasmid were used during transformation to replace the wild-type allele.

To create the *hsf1* (SAKL0A04576g) hypomorphic strains, we used the DAmP (decreased abundance by mRNA perturbation; Breslow *et al*, 2008) and decrease-of-function *hsf1* mutant (Sorger, 1990). In brief, the 475 bp DNA fragment of C-terminal-deleted (Δ460–557 aa) *hsf1* (SAKL0A04576g, +903 to +1,377 from ATG), a drug marker (KanMX6 or NatMX4), and the 355-bp 3' flanking region (+27 to +381 from the STOP codon) were PCR fused and used during transformation to replace the wild-type allele.

For mating-type switching from MATa to MATα, we again used the SAT1 flipper method. The 499-bp 5' flanking region of the MATα locus near the *DIC1* locus, together with the 3,206 bp fragment composed of the 2,587-bp MATα locus and the 619-bp 3' flanking regions of the *SLA2* locus, were ligated into pSFS2A vector between the KpnI-ApaI sites and NotI-SacII sites, respectively, to create the mating-type switching plasmid pSFS2A-5f-SkMATα-1. To transform cells, the KpnI-SacII-digested fragments from the pSFS2A-5f-SkMATα-1 plasmid were used.

To create the *IDH2* (SAKL0G03520g) promoter-LacZ plasmids, the promoter sequence (−437 to −1 from ATG of *IDH2*) was PCR amplified and cloned into the pRS41K-LacZ reporter plasmid between the KpnI-ApaI sites using by the In-Fusion method. The putative Azf1-binding site was deleted by using overlap-extension PCR-based mutagenesis. The promoter-LacZ strains of *IDH2* were created by transforming JYL1897 and SkAzf1HA1 with the corresponding plasmids. The transformants were selected in YPD + G418 medium.

All yeast transformations were performed by using electroporation and transformed cells were then selected as described previously (Hsu *et al*, 2021). Notably, since the *Candida albicans MAL2* promoter on the SAT1-FLIP cassette is leaky in *L. kluyveri*, the *L. kluyveri* SAT1-FLIP transformants could only be selected and propagated in YPD + Nou10 (10 µg/ml Nouseothricin) plates during strain construction procedures. The integrated SAT1-FLIP cassette

does not support efficient growth of *L. kluyveri cells* in liquid broth with Nouseothricin.

Media, important chemicals, and growth conditions

All media and chemicals used in this study are listed with abbreviations in Dataset EV14. All agar plates contained 2% agar. The basal YP (1% yeast extract and 2% peptone)-based media were sterilized by autoclaving, except for YPEtOH (YP + 2% ethanol). YPEtOH and all synthetic media were sterilized by filtering through 0.2 µm cup filters (Nalgene™ Rapid-Flow™ Sterile Single-Use Bottle Top Filters, 595–4,520; Thermo Fisher Scientific, USA). Some modifications to the recipes for synthetic media are noted in Dataset EV14. All cultures in culture tubes were grown on a drum roller rotating at 65–80 rpm. The normal growth temperature was 28–30°C. Heat stress was applied at 37–39°C, as indicated in the experiments.

Evolutionary repair experiments by suppressor development

The entire procedure is summarized in Appendix Fig S2. In detail, the MATa (SkSef1KChs3HA2) and MATα (SkSef1KChs3Hα1) *SEF1*-deleted founder strains (*sef1*Δ::KanMX6, *chs3*Δ::HphMX4, *ura3⁻*) were inoculated into a 20-ml YPD culture and grown at 30°C. After overnight growth, the cells were harvested and resuspended in 2 ml sterile ddH$_2$O at a cell density of ~40 OD$_{600}$/ml. Approximately 100–120 µl of cell suspensions containing 5 OD$_{600}$ cells (~10^8 CFU) were plated onto fresh YPGly plates, with 3–5 repeats per condition. The plates were incubated at 28, 37, 38, or 39°C. After 8 days, outcompeting colonies were re-streaked on YPGly plates and selected for another 5 days at 28, 37, 38, or 39°C, respectively. Only one large single colony was picked from each re-streaked population, and then the clones were streaked on YPD + HGB plates and incubated at 28°C for 2–3 days to confirm the original *chs3*Δ::hphMX4 genotype and to exclude contamination. The HGB-resistant clones were picked and inoculated into 1-ml YPD + G418/well cultures in U-shaped 96-deep-well plates (Nunc™ 96-Well Polypropylene Deep-Well™ Storage Plates, 278743, Thermo Fisher Scientific) covered with sterile breathable sealing film (BF-400-S, Axygen by Coring, USA). The deep-well plates were incubated with shaking (Micro-mixer MX4, FINEPCR, Korea) at 30°C for 24 h to amplify the cells, before confirming the original *sef1*Δ::KanMX6 genotype. The cells from saturated cultures were spun down and concentrated to ~130 µl, before adding 50 µl of 85% sterile glycerol and transferring them to 96-well plates (Tissue Culture Testplate 96 wells F-bottom, 92096, TPP, Switzerland) sealed with adhesive foil (UTI 3101, Smartgene by Ultra Violet, Taiwan) for −80°C storage.

Estimation of suppression rates

Suppression rates were estimated by performing a fluctuation analysis. To set up the primary culture, a single colony of each tested strain, the *SEF1*-deleted founder strain (SkSef1KChs3Hα1) and the control wild-type *SEF1* founder strain (SkChs3HA1), was inoculated into a 20 ml YPD culture and grown at 30°C. After 22 h of growth, the cells from the 1 ml culture were harvested and resuspended in sterile ddH$_2$O at a cell density of 1 OD$_{600}$/ml. The cell suspensions of primary cultures were then used to seed 32 independent secondary cultures (100 µl in 10-ml YPD, final 0.01 OD$_{600}$/ml, and 150 µl/

well) in U-shaped 96-deep-well plates (Nunc™ 96-Well Polypropyl-ene DeepWell™ Storage Plates, 278743, Thermo Fisher Scientific) covered with sterile breathable sealing film (BF-400-S, Axygen by Coring, USA). The deep-well plates were incubated with shaking (Micromixer MX4, FINEPCR, Korea) at 30°C to allow accumulation of adaptive mutations. After 20 h of growth, the cultures were harvested and 800-fold diluted in PBS. The cell densities were then estimated by using the Scepter™ Handheld Automated Cell Counter (PHCC00000, Millipore by Merck). The cells of each secondary cul-ture were diluted in sterile ddH$_2$O at a cell density of 1E+07 CFU/ ml. Cells suspensions were track plated (50 μl/track, 8 tracks/plate) onto YPGly plates (Square petri dish; D210-16, 100 × 100 × 15 mm, Simport Scientific) and incubated at 28 and 39°C for 7 days. Adap-tive (out-competing) colonies were counted and mutation rates were computed using the online Fluctuation AnaLysis CalculatOR "FALCOR" (https://lianglab.brocku.ca/FALCOR/; Hall *et al*, 2009). The results are displayed in Fig EV2.

The outcompeting clones evolved from the control wild-type *SEF1* founder strain (28 and 39°C-WT-Evo) were picked, purified, and stocked as described above with some modifications. Briefly, there were 20 clones picked, and the first 10 clones (clones 01 to 10) were picked from the same evolved population (the same track on the plate) while the other 10 clones (clones 11 to 20) were picked from independent populations (only one clone/track). Generally, we picked the biggest outcompeting colonies among the populations.

Genetic analyses by tetrad dissection

To mate yeast cells, 750 μl (~4 OD$_{600}$ containing ~1 × 10^8 CFU) each of MATa and MATα cells from YPD overnight cultures grown at 28°C for at least 20 h were mixed and harvested. The mixed-cell pel-lets were washed once with 1 ml sterile ddH$_2$O, resuspended in 10 μl sterile ddH$_2$O, and then spotted onto dry YPD plates. After growing at 28°C for 5–7 h, the cells from the spots were separated by streaking, and candidate zygotes were picked by using a Tetrad Dissection System [Nikon Eclipse 50i Microscope (Nikon, Japan) equipped with a TDM50™ Micromanipulator (Micro Video Instru-ments, Inc., USA) and a dissection needle (NDL-010, Singer Instru-ments, UK)]. The candidate zygotes were incubated on YPD plates at 28°C for 2–3 days and the heterozygous genotypes at the MAT loci were confirmed by gDNA extraction followed by PCR diagnosis for both MATa and MATα alleles.

For sporulation, 1 ml zygotes from YPD overnight culture were pelleted down, washed once with 1 ml sterile ddH$_2$O, and then inoc-ulated into 3 ml Spo medium (2% potassium acetate pH 9, optional: +1% adenine and 1% tryptophan) at 23–25°C. After 5–7 days, the asci from 50 μl sporulation culture were harvested, resuspended in 10 μl of 1 mg/ml zymolyase working solution diluted from 40 mg/ml zymolyase stock solution [Zymolyase® 100 T (07665–55, Nacalai Tesque Inc., Japan), 1× TE (10 mM Tris-Cl, 1 mM Na2EDTA pH 8), and 5% glucose] in sterile 1 M sorbitol or ddH$_2$O, and digested at room temperature for 5–8 min. The digested asci were streaked on dry YPD plates and the four spores from each tet-rad were picked and dissected onto the space of the same YPD plate. The dissected sister spore sets were incubated at 28°C for 2–3 days for further genotyping and phenotyping.

Notably, all strains used for tetrad dissection were in the *chs3Δ* background, which breaks the interspore bridges between sister

spores in asci (Coluccio & Neiman, 2004) and allows separation of sister spores, making *L. kluyveri* tetrad dissection achievable (Sigwalt *et al*, 2016).

Sanger sequencing for specific mutations on the *AZF1* and *IRA1* loci of the spores from tetrad dissection

To sequence the *AZF1* locus, the entire *AZF1* ORF (−21 from ATG to +17 from STOP) was PCR amplified using Phusion High-Fidelity DNA polymerase (F530L, Thermo Fisher Scientific) with the primer pair SkAzf1-UpATG-1 and SkAzf1-STOPdown-2 and an annealing temperature of 52°C. The product was purified by PCR cleanup using an AccuPrep® PCR/Gel Purification Kit (K-3037, Bioneer), before being subjected to Sanger sequencing with primer SkAzf1-555-1-seq 1 or SkAzf1-1151-1-seq 1. To sequence the *IRA1* locus, the second half of the *IRA1* ORF (+4,744 from ATG to +40 from STOP) was PCR amplified as detailed above, but with the primer pair SkIra1-4744-1-seq 1 and SkIra1-STOPdown-2 and an annealing tem-perature of 58°C, before undergoing purification and Sanger sequencing with primer SkIra1-5356-1-seq 1 or SkIra1-5946-1-seq 1. All primers used are listed in Dataset EV14. Notably, the *AZF1* and *IRA1* in JYL1897 (our lab parental strain) background carry.

Sanger sequencing for the whole *AZF1* and *IRA1* loci of the suppressor collections

The *AZF1* locus was sequenced as described above but the entire *AZF1* ORF was sequenced using seven sequencing primers. To sequence the *IRA1* locus, the first half (−25 to +4,854 from ATG) and the second half (+4,744 from ATG to +40 from STOP) of the *IRA1* ORF were PCR amplified as detailed above, with the primer pair SkIra1-UpATG-1 and SkIra1-4854-2-seq 1 and primer pair SkIra1-4744-1-seq 1 and SkIra1-STOPdown-2, respectively. The product was purified by PCR cleanup using a Zymo Genomic DNA clean & concentration™ kit-25 (Zymo Research, USA), before under-going Sanger sequencing with 17 sequencing primers. All primers used are listed in Dataset EV14.

Phenotypic assays

The spot assays, growth curve assays, and TTC reduction assays were performed as described previously (Hsu *et al*, 2021) with minor modifications. For the spot assays, cells grown in YPD over-night at 28°C were harvested by centrifugation (Eppendorf 5810R centrifuge; A-4-62 rotor; 1,500 *g*; 3 min; 25°C) and serially diluted to the desired cell density with sterile ddH$_2$O. Each dilution (10^7– 10^3 CFU/ml) was spotted onto agar plates (5 μl/spot, about 10^5– 10^1 CFU/spot) and incubated at 28°C or other temperatures as indi-cated. The plates were scanned using a scanner (Epson Perfection V800 Photo) and images were recorded after 3 days or as otherwise indicated.

For the growth curve assays, cells grown overnight in YPD (or other media as indicated) at 28°C were inoculated into 120 μl YPD medium in a 96-well plate (Tissue Culture Testplate 96 wells F-bottom, 92096, TPP) at a cell density of 0.2 OD$_{600}$/ml at indicated temperatures. Cell growth was measured at OD$_{595}$ in "2 × 2 multiple reads per well" mode every 12 min using a Tecan plate reader (Infi-nite 200 PRO, Tecan, Switzerland). Tecan software Magellan

Version 7.2 was used for data acquisition and analyses. For the Magellan method, we selected the plate definition "[TPP96ft]-Tecan Plastic Products AG6 Flat Transparent." Each 12 min cycle comprised 3 min reading, 1 min shaking, 3 min standing, 1 min shaking, 3 min standing, and 1 min shaking. For the glycolysis-inhibited medium, 0.1% 2-deoxy-D-glucose (D8375, Sigma) was added to the YPD medium. For amino acid pre-starvation, we used SM + 2X Ura medium (SM supplemented with 80 mg/l uracil) given that we employed ura^- strains in this study. Pre-starvation was performed by inoculating a single colony from a YPD plate into a 5-ml SM + 2X Ura culture and allowing it to grow for 23 h at 28°C. For cell density-dependent growth assays, growth curves using different initial cell densities (0.005, 0.01, 0.02, 0.05, 0.1, or 0.2 OD_{600}/ml) in YPD were measured for 24 h at 28, 37, or 39°C. Maximal growth rates were determined by calculating the maximum slope of each growth curve based on 30–40 time points in Magellan software, as illustrated in Appendix Fig S1C.

For the epistasis analysis, the growth curve assays were used as described above with modifications. Briefly, two initial cell densities (0.01 and 0.4 OD_{600}/ml) were used to keep or eliminate the cell density effect of $azf1\Delta$. Maximal growth rates from three technical repeats were determined by calculating the maximum slope of each growth curve based on 10 time points in Magellan software. The relative fitness was calculated by comparing it to the wild-type and displayed as %. The epistasis status was determined by using the multiplicative model (van Leeuwen et al, 2017), which suggests that the genotype with a pair of loci has fitness values equal to the product of fitness values at the two different loci if there is no epistasis between them.

For the desiccation assays, a single colony of each tested strain was inoculated in 3 ml YPD and grown at 28°C for 20 h. Cells were then harvested and diluted at cell densities of 1 OD_{600}/ml with sterile ddH_2O. Two 1 ml aliquots (containing ~10^7 CFU) were made for each tested strain in 1.5 ml tubes. The desiccated sample was prepared by spinning down cells, removing supernatants, sealing the opened tube with a sterile breathable sealing film (BF-400-S, AXYGEN, USA), and air-drying the cell pellets at 28°C for 20 h. The control samples were prepared by retaining the supernatants and keeping the tubes capped. After 20 h, the cells were rehydrated in 1 ml sterile ddH_2O for 1 h. The viability was determined qualitatively by spot assays on YPD plates as described above after 3 days of incubation at 28°C. The desiccation sensitivity was used to represent the severity of $ira1$ loss-of-function mutations or other mutations generating the same effect as $ira1$ loss-of-function does.

For the TTC reduction assays, cells grown overnight in YPD at different temperatures as indicated were harvested and diluted to a cell density of 1 OD_{600}/ml in sterile ddH_2O. Then, 5 µl of each cell suspension (~10^5 CFU) was spotted on YPGly plates. The plates were incubated at 28°C for 2 days, and before being overlaid with 20 ml melted TTC agar (0.1% TTC, 2% agar in sterile PBS [8 g/l NaCl, 0.2 g/l KCl, 1.44 g/l Na_2HPO_4, and 0.24 g/l KH_2PO_4 pH 7.4]), it was allowed to solidify for 20 min at room temperature. The plates were incubated at 28°C for red color development. The plates were scanned after 2.5, 8, and 24 h of color development using a scanner (Epson Perfection V800 Photo).

For the Phloxine B permeability assays, cells grown overnight in YPD at 28°C were harvested by centrifugation (Eppendorf 5810R centrifuge; A-4-62 rotor; 1,500 g; 3 min; 25°C) and diluted to a cell density of 1 OD_{600}/ml in sterile ddH_2O. Then, 5 µl of each cell suspension (~10^5 CFU) was spotted on YPD plates containing 5 µg/ml Phloxine B (P4030, Sigma). The plates were incubated at 28 or 39°C and scanned after 3 days of pink color development using a scanner (Epson Perfection V800 Photo). To intensify differences in color, the images were processed uniformly by increasing contrast and brightness by 40%.

For the cell wall disruption sensitivity assays, cells grown in YPD for 16 h at 28°C were harvested and re-inoculated into 5 ml of YPD at a cell density of 0.2 OD_{600}/ml for 24 h at 28 or 39°C. The cells were harvested by centrifugation (Eppendorf 5810R centrifuge; A-4-62 rotor; 1,500 g; 3 min; 25°C) and diluted at cell densities of 0.6 OD_{600}/ml with 1 ml of pH 7.6 Tris-Cl buffer containing 60 units/ml Zymolyase® 100T (07665–55, Nacalai Tesque Inc.) in a disposable 2 ml photometer cuvette (112117, LP Italiana SPA, Italy). The cell walls were digested initially for 2 h in the Zymolase-hosting buffer, before further digestion using 0.1% SDS at room temperature, with gentle pipetting every 30 min. OD_{600} at 0, 2, 4, and 22 h was measured using a Beckman DU® 800 UV/Visible spectrophotometer (Beckman Coulter, USA) to evaluate intact cells. Cells with disrupted cell walls lyse in the presence of SDS due to hypoosmolarity, reducing the OD_{600} value in the cell suspension. The ratio of OD_{600} at each time point relative to time 0 (0 h) was calculated to represent sensitivity to cell wall disruption, with a lower ratio reflecting higher sensitivity.

For the cooperative growth assays in liquid broths (Appendix Fig S16A), cells grown overnight in YPD (20 h) at 28°C were harvested and diluted to a cell density of 1 OD_{600}/ml in sterile ddH_2O. For the "independent cultures," AZF1 (reference strain, HGB-sensitive) and $azf1\Delta$ (test strain, HGB-resistant) cell suspensions were diluted independently to a cell density of 0.01 and 0.05 OD_{600}/ml, respectively, in a 1 ml YPD culture. For the "co-culture," the AZF1 and $azf1\Delta$ cell suspensions were mixed at cell densities of 0.01 and 0.05 OD_{600}/ml, respectively, in the same 1 ml YPD culture. Cell growth was measured at 39°C using a Tecan plate reader (Infinite 200 PRO, Tecan), as described above. After 20 h of growth, 50 µl of each of the "independent cultures" was mixed and resuspended in 900 µl sterile ddH_2O, and then 100 µl of the "co-culture" was resuspended in 900 µl sterile ddH_2O. Two suspensions (~0.4 OD_{600}/ml) were serially diluted and plated onto YPD plates at an estimated density of ~10^2 CFU/plate. The YPD plates were incubated at 28°C for 2 days, before being replicated onto YPD + HGB plates and incubated for 1 day. The ratio of $azf1\Delta$ ($CFU^{HGB-resistant}$)-to-AZF1 (total CFU^{YPD} – $CFU^{HGB-resistant}$) cells was calculated from six technical repeats.

For the cooperative growth assays on agar plates (Appendix Fig S16C), cells grown overnight in YPD (20 h) at 28°C were harvested and diluted in sterile ddH_2O at cell densities of 1 OD_{600}/ml for the wild-type and 5 OD_{600}/ml for the $azf1\Delta$ mutant (to detect the cooperative growth, more cells of the $azf1\Delta$ mutant than the wild-type needed to be used due to the fitness difference between these two strains under the tested condition). For the "independent cultures," 5 µl of the wild-type (reference strain, HGB sensitive, ~10^5 CFU) and $azf1\Delta$ (test strain, HGB resistant, ~5×10^5 CFU) cell suspensions were spotted independently onto a YPD plate. For the "co-culture," 5 µl of the mixed wild-type and $azf1\Delta$ cell suspension containing the same CFU as described above were spotted onto the same YPD plate. After incubation at 39°C for

3 days, 7 × 7 mm areas of gel-hosting cell colonies were sliced out and rehydrated with 1 ml sterile ddH$_2$O at room temperature. After 1 h, the cells were washed down five times by means of mild-pulse vortexing. Suspensions were transferred to new 2 ml tubes and the wash step was repeated. The new suspensions were combined with the previous ones. Two slices from the "independent cultures" were rehydrated and resuspended together, whereas only one slice from the "co-culture" was processed. Two suspensions (~3 OD$_{600}$/ml for the "independent culture" and ~1.6 OD$_{600}$/ml for the "co-culture") were then serially diluted and drop plated. Each dilution (10^6–10^3 CFU/ml) was spotted onto the YPD and YPD + HGB plates (5 μl/spot, ~10^4–10^1 CFU/spot) and incubated at 28°C for 2–3 days. Spots with < 50 CFU were counted. Notably, instead of using the HGB resistant to HGB-sensitive ratio, we used the frequency of *azf1Δ* cells (CFU$^{HGB-resistant}$/total CFU^{YPD}) to represent the level of cooperative growth, thereby reducing technical variations caused by the considerable difference in viability between *AZF1* and *azf1Δ* cells on agar plates. The frequencies were calculated from six technical repeats. Due to their lower fitness at 39°C, for cases in the *sef1Δ* background (*sef1Δ*, HGB-sensitive; *sef1Δazf1Δ*, HGB-resistant), the cell densities of initial cell suspensions were modified to 2 OD$_{600}$/ml for the *sef1Δ* mutant and 4 OD$_{600}$/ml for the *sef1Δazf1Δ* mutant.

Beta-galactosidase assays

LacZ expression levels for the one-hybrid assays were quantified using liquid β-galactosidase assays, as described previously but with some modifications (Hsu *et al*, 2021). In brief, early log-phase (0.5–1.0 OD$_{600}$/ml) cells cultured in indicated media were assayed. All subcultures were initiated with 0.2 OD$_{600}$/ml of inoculum from overnight-grown cells. One-hybrid strains from the chromosome-integrated system were subcultured for 4.5 h, whereas the strains from the plasmid-based system were subcultured for 5.5 h in the presence of 200 μg/ml HGB. Due to the relatively weak activation of Azf1, more cells (~1 OD$_{600}$ cells) per reaction and a longer incubation time (90 min) at 37°C were required for colorimetric reactions. LacZ levels are displayed as Miller units.

Genomic DNA extraction for whole-genome sequencing

Pure genomic DNA was extracted via the phenol–chloroform method, followed by RNase treatment, as described previously but with modifications (Hsu *et al*, 2011). In brief, ~100 OD$_{600}$ cells (from a 20 ml YPD overnight culture) per sample were extracted. The cells were resuspended in 200 μl gDNA lysis buffer [2% Triton X-100, 1% SDS, 100 mM NaCl, 10 mM Tris-Cl (pH 8), and 1 mM Na$_2$EDTA] and transferred into a 2 ml breaking tube (72.693, Sarstedt) containing 250 μl PCIA (phenol:chloroform:isoamyl alcohol = 25:24:1, 0.1% 8-quinolinol, pH 8) and a 500 μl volume of glass beads (11079105, BioSpec Products). The cells were lysed by using a FastPrep-24™ 5G Homogenizer (MP Biomedicals™) at a speed of 6 m/s for 40 s. The aqueous phases were then extracted again using 200 μl PCIA (pH 8). RNase treatment involved adding 10 μl of 10 mg/ml RNase A (R5503, Sigma) into a 400 μl nucleic acid suspension in TE buffer (10 mM Tris-Cl and 1 mM Na$_2$EDTA, pH 8) and incubating at 37°C for 1 h. The crude gDNA was then precipitated by adding 1 ml of 99% ethanol with 20 μl of 3 M sodium

acetate (pH 5.2), followed by mild mixing for 30 min. The nucleic acid pellets were rehydrated in 200 μl ddH$_2$O at 65°C for 10 min and then purified again by using a Zymo Genomic DNA clean & concentration™ kit-25 (Zymo Research, USA) to remove the small DNA fragments. All procedures followed the manufacturer's instructions, but with the modification of a two-cycle wash step using 500 μl wash buffer. The final gDNA was eluted with 50 μl of 65°C elution buffer. DNA concentrations were measured using a Qubit™ dsDNA BR Assay Kit (Q32853, Invitrogen by Thermo Fisher Scientific). The quality of the gDNA was checked using the 2200 TapeStation system (G2964AA), Genomic DNA ScreenTape (5,067–5,365), and Genomic DNA Reagents (5,067–5,366) obtained from Agilent Technologies.

DNA-seq analyses

Isolated genomic DNAs were fragmented using a Covaris M220 Focused-ultrasonicator (Covaris, USA), and DNA libraries were prepared using a Truseq DNA PCR-free HT kit (Illumina, USA). Two founders and 12 suppressor clones were sequenced to an estimated average depth of 50-fold coverage by paired-end 150 bp read length following the protocol of the NextSeq 500 Mid output v2 (300 cycles) sequencing kit on an Illumina NextSeq 500 System controlled by the NextSeq Control Software (NCS v2.2.0, Illumina). Real-Time Analysis (RTA v2.4.11, Illumina) software was used to generate the BCL files containing base calls and associated quality scores (Q-scores). The bcl2fastq Conversion Software (v2.17, Illumina) was used to demultiplex sequencing data and convert the BCL files into FASTQ files, which were then processed by FastQC (www.bioinformatics.babraham.ac.uk/projects/fastqc) and summarized in MultiQC (Ewels *et al*, 2016) to generate a QC report for comparison.

Raw reads were mapped to the reference CBS 3082 genome using the Burrows–Wheeler Aligner (BWA, v0.7.17) and the BWA-MEM algorithm (Li & Durbin, 2009; preprint: Li, 2013) with default parameters to obtain the BAM files. Mapping rates and sequencing coverages were determined in Samtools v1.9 (Li *et al*, 2009). Variant calling was performed on the BAM files using GATK v4.1.2.0 (McKenna *et al*, 2010). According to "hard-filtering" recommendations for germline short variant (SNP and INDEL) discovery described in the GATK website (https://gatk.broadinstitute.org/hc/en-us/), we applied the following filtering settings with some modifications for SNP calling: "QD < 2.0 ‖ FS > 60.0 ‖ MQ < 40.0 ‖ MQRankSum < -12.5 ‖ ReadPosRankSum < -8.0 ‖ SOR > 4.0," and for INDEL calling: "QD < 2.0 ‖ FS > 200.0 ‖ ReadPosRankSum < -20.0," to obtain VCF files. Only variants existing in the suppressor clones but not in their founder strain were retained for subsequent analyses. The suppressor-unique variants were then filtered according to sequencing depth (DP) > 20 and allele frequency (AF) ≥ 0.5 to get the final variant spectra. SnpEff v4.3t (Cingolani *et al*, 2012) was used to annotate and predict the effects of suppressor-unique variants on genes. The final unique variants with annotations are listed in Dataset EV4.

RNA extraction and DNase treatment

Approximately 10 OD$_{600}$ of early log-phase (0.5–1.0 OD$_{600}$/ml) cells from subcultures grown from 0.2 OD$_{600}$/ml of inoculum for 5.5 h under the indicated conditions were harvested. Total RNA was extracted by means of the phenol–chloroform method and treated

with the TURBO DNA-free™ kit (AM1907, Ambion, Invitrogen by Thermo Fisher Scientific), as described (Hsu *et al*, 2021) but with small modifications. In brief, the cells were resuspended in 500 μl nuclease-free and ice-cold RNA lysis buffer and then transferred into a 2 ml breaking tube (72.693, Sarstedt, Germany) containing 250 μl ice-cold acidic PCIA and a 500 μl volume of glass beads (11079105, BioSpec Products, USA). The cells were lysed using a FastPrep-24™ 5G Homogenizer (MP Biomedicals™, USA) at a speed of 6 m/s for 40 s at room temperature. The aqueous phases were then extracted by two rounds of 200 μl ice-cold acidic PCIA treatment, and the nucleic acids were obtained after 2 h of ethanol precipitation. RNA quality was checked using a Bioanalyzer 2100 instrument (Agilent Technologies, USA) with an RNA 6000 Nano LabChip kit (Agilent Technologies). The DNase-treated RNAs were stored at 80°C for further RT–qPCR or RNA-seq analyses.

Reverse transcription (RT) and quantitative-PCR (qPCR) analyses

RT–qPCR was performed as described previously but with some modifications (Hsu *et al*, 2021). In brief, cDNA synthesis was conducted in the presence of different rRNasin® Ribonuclease Inhibitors (N2511, Promega, USA) at a concentration of 1 μl per 20-μl reaction. qPCR was performed using the model QuantStudioTM 12 K Flex Real-Time PCR System (Applied Biosystems by Thermo Fisher Scientific). Primers used for qPCR are listed in Dataset EV14. *L. kluyveri CDC34* transcripts (SAKL0D02530g) were used as an endogenous control for qPCR. The average $\Delta\Delta C_T$ and standard deviation were determined from at least three technical repeats. The relative fold change of each gene is shown according to the $2^{-\Delta\Delta C_T}$ method.

RNA-seq analyses

For each strain and condition, total RNA was extracted from three biological replicates. RNA-seq libraries were prepared using a TruSeq Stranded mRNA HT Sample Prep Kit (Illumina) on 2 μg total RNA and sequenced by single-end 75 bp read length following the protocol of the NextSeq 500 High Output kit v2.5 (75 cycles) sequencing kit on an Illumina NextSeq 500 System. Total read numbers were estimated to be 20 million reads per sample. Raw reads were quality trimmed using Trimmomatic v0.38 (Bolger *et al*, 2014) with options: "ILLUMINACLIP:2:30:10 LEADING:3 TRAILING:3 SLIDINGWINDOW:4:15 MINLEN:36." The relative abundance of each gene in units of transcripts per million (TPM) for each sample was quantified using Salmon v1.4.0 (Patro *et al*, 2017) with options: "--numBootstraps 200 --validateMappings –gcBias." Tximport (Soneson *et al*, 2015) by default was used to convert the estimated transcript abundance files from Salmon to a DESeq2-compatible dataset. DESeq2 (Love *et al*, 2014) was used for the analysis of differential gene expression in R v4.0.4 with default settings. In DESeq2, the *P*-values attained by the Wald test were corrected for multiple testing using the Benjamini and Hochberg method. Genes with mean TPM < 1 under all conditions were omitted from our analyses. Differences in gene expression with adjusted *P*-values < 0.05 and fold-change of at least two were considered significantly different. All results in the standard DESeq2 output format and the TPM of each gene from three technical repeats are presented in Datasets EV1, EV2, and EV5–EV12.

The heatmaps of selected gene expressions were created using the mean TPM ratio relative to a reference sample, as indicated. The green–white–red color scale ranging from the 5th to 90th percentiles of the selected values was generated in Excel 2016 using the conditional formatting function. The white color represents the median with a value of ~1, indicating no differential expression.

Gene ontology (GO) enrichment analyses and manual simplification

For *L. kluyveri* GO analyses, gene ontology information borrowed from *S. cerevisiae* (SGD, http://www.yeastgenome.org; GO Term Finder, version 0.86) was used to analyze the *L. kluyveri* genes. In brief, the *L. kluyveri* genes were converted to *S. cerevisiae* orthologs using a published Lk-to-Sc cross-reference table of orthology (Hsu *et al*, 2021). *L. kluyveri* genes in the input list without a clear *S. cerevisiae* ortholog (~10%) were omitted from our GO enrichment analyses of "biological processes." The enriched GO terms with adjusted *P*-values < 0.01 were considered significant (a more stringent cut-off for *P*-values generally did not affect the results of subsequent analyses). We did not correct the genetic background because *L. kluyveri* and *S. cerevisiae* share similar gene numbers in their genomes (~6,000 genes). To browse the GO hierarchy, the enriched GO terms from each set of differentially expressed genes were placed on the QuickGo website (Binns *et al*, 2009). To "simplify" the enriched GO term list, the resolved GO terms were checked manually and the broader parent terms were removed, while the more specific child terms close to the leaf node of the hierarchy tree were retained to assist in simplifying functional annotations.

Protein extraction and Western blotting

Total protein was extracted by using the NaOH/TCA/HU method with modifications (Lu *et al*, 2016). In brief, ~3 OD_{600} cells were resuspended in 1 ml lysis buffer (0.185 M NaOH, 0.75% β-ME) and lysed on ice for 10 min. Next, we added 150 μl of 55% trichloroacetic acid (TCA, T9159, Sigma, USA) to the lysis suspension at a final percentage of 8% to precipitate proteins. After 15 min on ice, the precipitants were spun down by centrifugation (Eppendorf 5424R centrifuge; FA-45-24-11 rotor; 13 K rpm; 10 min; 4°C) and the supernatant was discarded. The centrifugation step was repeated to remove all residual supernatant. Then, we added 300 μl of high urea (HU) sample buffer (8 M Urea, 5% SDS, 0.2 M Tris–HCl pH 6.5, 1 mM Na_2EDTA, and 0.01% bromophenol blue) supplemented with 2 M Tris base in a 50-to-3 ratio to the protein pellets, and then incubated them at 65°C for at least 40 min, before subjecting them to vigorous pipetting to sufficiently dissolve the pellets.

Protein extracts were resolved by 8% SDS–PAGE (Sambrook, 2001) under a constant voltage of 80 V for 40 min of stacking followed by 150 V for 2 h of separating, before being blotted onto an Immobilon®-P PVDF Membrane (IPVH00010, Millipore by Merck) in a transfer buffer (25 mM Tris base, 192 mM glycine, and 20% methanol) under a constant voltage of 30 V for 20 h of transfer at 4°C. Post-transfer membranes were then blocked with the blocking buffer [1% casein (C5890, Sigma) in PBST (1% Tween® 20 in 1× PBS)] for 1 h. For immunodetection, rabbit polyclonal anti-TAP antibody (CAB1001, Thermo Fisher Scientific) diluted 1:2,000 in blocking buffer was used to detect TAP-tagged

Sef1 and Azf1. Alpha-tubulin was used as an internal control and it was detected by means of rabbit monoclonal antibody (ab184970, Abcam, UK) diluted 1:20,000 in blocking buffer. The blots were hybridized with each primary antibody for 2 h at room temperature and washed three times with PBST (5 min each). Finally, the blot was hybridized with Peroxidase-AffiniPure Donkey Anti-Rabbit IgG secondary antibody (711-035-152, Jackson ImmunoResearch, USA) diluted 1:20,000 in blocking buffer for 1 h at room temperature, and then washed three times with PBST. Chemiluminescence was developed with enhanced ECL reagents (NEL105001EA, PerkinElmer, USA) and visualized by exposure to an X-ray film. Band intensity was quantified by ImageJ software (https://imagej.nih.gov/ij/index.html; Schneider *et al*, 2012).

Statistical analysis

Details of statistical analyses are presented in the main text or corresponding figure legends. Statistical significance was established using the unpaired Student's *t*-test or the one-sample *t*-test in Excel 2016 or the default functions packaged in each analysis tool.

Data availability

The datasets produced in this study are available in the following databases:

- RNA-seq data: Gene Expression Omnibus database GSE200532 (https://www.ncbi.nlm.nih.gov/geo/query/acc.cgi?acc=GSE200532). The processed results are shown in Datasets EV1, EV2, and EV5–EV12.
- DNA-seq data: NCBI BioProject database PRJNA825358 (https://www.ncbi.nlm.nih.gov/bioproject/term=PRJNA825358). The processed results are shown in Dataset EV4.

Expanded View for this article is available online.

Author contributions
Po-Chen Hsu: Conceptualization; data curation; formal analysis; validation; investigation; visualization; methodology; writing – original draft; writing – review and editing. **Yu-Hsuan Cheng:** Data curation; formal analysis; methodology; writing – original draft. **Chia-Wei Liao:** Data curation; formal analysis; methodology; writing – original draft. **Richard Ron R Litan:** Data curation; formal analysis; investigation; visualization. **Yu-Ting Jhou:** Formal analysis; investigation; visualization. **Florica Jean Ganaden Opoc:** Investigation; visualization. **Ahmed A A Amine:** Investigation. **Jun-Yi Leu:** Conceptualization; resources; supervision; funding acquisition; investigation; writing – original draft; project administration; writing – review and editing.

Disclosure and competing interests statement
The authors declare that they have no conflict of interest.

References

Aggeli D, Li Y, Sherlock G (2021) Changes in the distribution of fitness effects and adaptive mutational spectra following a single first step towards adaptation. *Nat Commun* 12: 5193

Amine AAA, Liao C-W, Hsu P-C, Opoc FJG, Leu J-Y (2021) Experimental evolution improves mitochondrial genome quality control in *Saccharomyces cerevisiae* and extends its replicative lifespan. *Curr Biol* 31: 3663–3670

Ayala FJ, Campbell CA (1974) Frequency-dependent selection. *Annu Rev Ecol Syst* 5: 115–138

Barrick JE, Lenski RE (2013) Genome dynamics during experimental evolution. *Nat Rev Genet* 14: 827–839

Barrick JE, Kauth MR, Strelioff CC, Lenski RE (2010) *Escherichia coli* rpoB mutants have increased evolvability in proportion to their fitness defects. *Mol Biol Evol* 27: 1338–1347

Bedford T, Hartl DL (2009) Optimization of gene expression by natural selection. *Proc Natl Acad Sci USA* 106: 1133–1138

Beese SE, Negishi T, Levin DE (2009) Identification of positive regulators of the yeast Fps1 Glycerol Channel. *PLoS Genet* 5: e1000738

Binns D, Dimmer E, Huntley R, Barrell D, O'Donovan C, Apweiler R (2009) QuickGO: a web-based tool for gene ontology searching. *Bioinformatics* 25: 3045–3046

Blundell JR, Schwartz K, Francois D, Fisher DS, Sherlock G, Levy SF (2019) The dynamics of adaptive genetic diversity during the early stages of clonal evolution. *Nat Ecol Evol* 3: 293–301

Bolger AM, Lohse M, Usadel B (2014) Trimmomatic: a flexible trimmer for Illumina sequence data. *Bioinformatics* 30: 2114–2120

Breslow DK, Cameron DM, Collins SR, Schuldiner M, Stewart-Ornstein J, Newman HW, Braun S, Madhani HD, Krogan NJ, Weissman JS (2008) A comprehensive strategy enabling high-resolution functional analysis of the yeast genome. *Nat Methods* 5: 711–718

Brion C, Pflieger D, Friedrich A, Schacherer J (2015) Evolution of intraspecific transcriptomic landscapes in yeasts. *Nucleic Acids Res* 43: 4558–4568

Butler G, Kenny C, Fagan A, Kurischko C, Gaillardin C, Wolfe KH (2004) Evolution of the MAT locus and its Ho endonuclease in yeast species. *Proc Natl Acad Sci USA* 101: 1632–1637

Carroll SB (2000) Endless forms: the evolution of gene regulation and morphological diversity. *Cell* 101: 577–580

Cazzanelli G, Pereira F, Alves S, Francisco R, Azevedo L, Dias Carvalho P, Almeida A, Côrte-Real M, Oliveira MJ, Lucas C *et al* (2018) The yeast *Saccharomyces cerevisiae* as a model for understanding RAS proteins and their role in human tumorigenesis. *Cell* 7: 14

Chen P, Zhang J (2020) Antagonistic pleiotropy conceals molecular adaptations in changing environments. *Nat Ecol Evol* 4: 461–469

Cingolani P, Platts A, Wang LL, Coon M, Nguyen T, Wang L, Land SJ, Lu X, Ruden DM (2012) A program for annotating and predicting the effects of single nucleotide polymorphisms, SnpEff. *Fly* 6: 80–92

Coluccio A, Neiman AM (2004) Interspore bridges: a new feature of the *Saccharomyces cerevisiae* spore wall. *Microbiology* 150: 3189–3196

Conrad M, Schothorst J, Kankipati HN, Van Zeebroeck G, Rubio-Texeira M, Thevelein JM (2014) Nutrient sensing and signaling in the yeast *Saccharomyces cerevisiae*. *FEMS Microbiol Rev* 38: 254–299

Coolon JD, McManus CJ, Stevenson KR, Graveley BR, Wittkopp PJ (2014) Tempo and mode of regulatory evolution in *Drosophila*. *Genome Res* 24: 797–808

Dalal CK, Johnson AD (2017) How transcription circuits explore alternative architectures while maintaining overall circuit output. *Genes Dev* 31: 1397–1405

Dittmar EL, Oakley CG, Conner JK, Gould BA, Schemske DW (2016) Factors influencing the effect size distribution of adaptive substitutions. *Proc R Soc B Biol Sci* 283: 20153065

Ewels P, Magnusson M, Lundin S, Käller M (2016) MultiQC: summarize analysis results for multiple tools and samples in a single report. *Bioinformatics* 32: 3047–3048

Garland T (2014) Trade-offs. *Curr Biol* 24: R60–R61

Gasch AP, Spellman PT, Kao CM, Carmel-Harel O, Eisen MB, Storz G, Botstein D, Brown PO (2000) Genomic expression programs in the response of yeast cells to environmental changes. *Mol Biol Cell* 11: 4241–4257

Génolevures Consortium, Souciet J-L, Dujon B, Gaillardin C, Johnston M, Baret PV, Cliften P, Sherman DJ, Weissenbach J, Westhof E *et al* (2009) Comparative genomics of protoploid Saccharomycetaceae. *Genome Res* 19: 1696–1709

Gerrish PJ, Lenski RE (1998) The fate of competing beneficial mutations in an asexual population. *Genetica* 102–103: 127–144

Goncalves A, Leigh-Brown S, Thybert D, Stefflova K, Turro E, Flicek P, Brazma A, Odom DT, Marioni JC (2012) Extensive compensatory cis-trans regulation in the evolution of mouse gene expression. *Genome Res* 22: 2376–2384

Gorter de Vries AR, Voskamp MA, van Aalst ACA, Kristensen LH, Jansen L, van den Broek M, Salazar AN, Brouwers N, Abeel T, Pronk JT *et al* (2019) Laboratory evolution of a *Saccharomyces cerevisiae* × *S. eubayanus* hybrid under simulated lager-brewing conditions. *Front Genet* 10: 242

Grosfeld EV, Bidiuk VA, Mitkevich OV, Ghazy ESMO, Kushnirov VV, Alexandrov AI (2021) A systematic survey of characteristic features of yeast cell death triggered by external factors. *J Fungi* 7: 886

Hall BM, Ma C-X, Liang P, Singh KK (2009) Fluctuation AnaLysis CalculatOR: a web tool for the determination of mutation rate using Luria–Delbrück fluctuation analysis. *Bioinformatics* 25: 1564–1565

Ho Y-H, Gasch AP (2015) Exploiting the yeast stress-activated signaling network to inform on stress biology and disease signaling. *Curr Genet* 61: 503–511

Hodgins-Davis A, Rice DP, Townsend JP (2015) Gene expression evolves under a house-of-cards model of stabilizing selection. *Mol Biol Evol* 32: 2130–2140

Hsu P-C, Yang C-Y, Lan C-Y (2011) *Candida albicans* Hap43 is a repressor induced under low-iron conditions and is essential for iron-responsive transcriptional regulation and virulence. *Eukaryot Cell* 10: 207–225

Hsu P-C, Lu T-C, Hung P-H, Jhou Y-T, Amine AAA, Liao C-W, Leu J-Y (2021) Plastic rewiring of Sef1 transcriptional networks and the potential of nonfunctional transcription factor binding in facilitating adaptive evolution. *Mol Biol Evol* 38: 4732–4747

Huang C-J, Lu M-Y, Chang Y-W, Li W-H (2018) Experimental evolution of yeast for high-temperature tolerance. *Mol Biol Evol* 35: 1823–1839

Jamnik P, Medved P, Raspor P (2006) Increased glutathione content in yeast *Saccharomyces cerevisiae* exposed to NaCl. *Ann Microbiol* 56: 175–178

Jerison ER, Kryazhimskiy S, Mitchell JK, Bloom JS, Kruglyak L, Desai MM (2017) Genetic variation in adaptability and pleiotropy in budding yeast. *Elife* 6: e27167

Johnson AD (2017) The rewiring of transcription circuits in evolution. *Curr Opin Genet Dev* 47: 121–127

Johnson MS, Gopalakrishnan S, Goyal J, Dillingham ME, Bakerlee CW, Humphrey PT, Jagdish T, Jerison ER, Kosheleva K, Lawrence KR *et al* (2021) Phenotypic and molecular evolution across 10,000 generations in laboratory budding yeast populations. *Elife* 10: e63910

Kao KC, Sherlock G (2008) Molecular characterization of clonal interference during adaptive evolution in asexual populations of *Saccharomyces cerevisiae*. *Nat Genet* 40: 1499–1504

Kinsler G, Geiler-Samerotte K, Petrov DA (2020) Fitness variation across subtle environmental perturbations reveals local modularity and global pleiotropy of adaptation. *Elife* 9: e61271

Kvitek DJ, Sherlock G (2013) Whole genome, whole population sequencing reveals that loss of signaling networks is the major adaptive strategy in a constant environment. *PLoS Genet* 9: e1003972

LaBar T, Phoebe Hsieh Y-Y, Fumasoni M, Murray AW (2020) Evolutionary repair experiments as a window to the molecular diversity of life. *Curr Biol* 30: R565–R574

Laman Trip DS, Youk H (2020) Yeasts collectively extend the limits of habitable temperatures by secreting glutathione. *Nat Microbiol* 5: 943–954

Lang GI, Rice DP, Hickman MJ, Sodergren E, Weinstock GM, Botstein D, Desai MM (2013) Pervasive genetic hitchhiking and clonal interference in forty evolving yeast populations. *Nature* 500: 571–574

Laussel C, Léon S (2020) Cellular toxicity of the metabolic inhibitor 2-deoxyglucose and associated resistance mechanisms. *Biochem Pharmacol* 182: 114213

Lavoie H, Hogues H, Mallick J, Sellam A, Nantel A, Whiteway M (2010) Evolutionary tinkering with conserved components of a transcriptional regulatory network. *PLoS Biol* 8: e1000329

Lee KS, Irie K, Gotoh Y, Watanabe Y, Araki H, Nishida E, Matsumoto K, Levin DE (1993) A yeast mitogen-activated protein kinase homolog (Mpk1p) mediates signalling by protein kinase C. *Mol Cell Biol* 13: 3067–3075

Levy SF, Blundell JR, Venkataram S, Petrov DA, Fisher DS, Sherlock G (2015) Quantitative evolutionary dynamics using high-resolution lineage tracking. *Nature* 519: 181–186

Li H (2013) Aligning sequence reads, clone sequences and assembly contigs with BWA-MEM. *arXiv* https://doi.org/10.48550/arXiv.1303.3997 [PREPRINT]

Li H, Durbin R (2009) Fast and accurate short read alignment with burrows–wheeler transform. *Bioinformatics* 25: 1754–1760

Li H, Johnson AD (2010) Evolution of transcription networks—lessons from yeasts. *Curr Biol* 20: R746–R753

Li H, Handsaker B, Wysoker A, Fennell T, Ruan J, Homer N, Marth G, Abecasis G, Durbin R, 1000 Genome Project Data Processing Subgroup (2009) The sequence alignment/map format and SAMtools. *Bioinformatics* 25: 2078–2079

Li Y, Venkataram S, Agarwala A, Dunn B, Petrov DA, Sherlock G, Fisher DS (2018) Hidden complexity of yeast adaptation under simple evolutionary conditions. *Curr Biol* 28: 515–525

Love MI, Huber W, Anders S (2014) Moderated estimation of fold change and dispersion for RNA-seq data with DESeq2. *Genome Biol* 15: 550

Lu Y-J, Swamy KBS, Leu J-Y (2016) Experimental evolution reveals interplay between Sch9 and Polyploid stability in yeast. *PLoS Genet* 12: e1006409

Lynch M, Field MC, Goodson HV, Malik HS, Pereira-Leal JB, Roos DS, Turkewitz AP, Sazer S (2014) Evolutionary cell biology: two origins, one objective. *Proc Natl Acad Sci USA* 111: 16990–16994

Mack KL, Nachman MW (2017) Gene regulation and speciation. *Trends Genet* 33: 68–80

Mazáň M, Mazáňová K, Farkaš V (2008) Phenotype analysis of *Saccharomyces cerevisiae* mutants with deletions in Pir cell wall glycoproteins. *Antonie Van Leeuwenhoek* 94: 335–342

McCloskey D, Xu S, Sandberg TE, Brunk E, Hefner Y, Szubin R, Feist AM, Palsson BO (2018) Evolution of gene knockout strains of *E. coli* reveal regulatory architectures governed by metabolism. *Nat Commun* 9: 3796

McDonald MJ (2019) Microbial experimental evolution – a proving ground for evolutionary theory and a tool for discovery. *EMBO Rep* 20: e46992

McKenna A, Hanna M, Banks E, Sivachenko A, Cibulskis K, Kernytsky A, Garimella K, Altshuler D, Gabriel S, Daly M *et al* (2010) The genome analysis toolkit: a MapReduce framework for analyzing next-generation DNA sequencing data. *Genome Res* 20: 1297–1303

Mérot C, Llaurens V, Normandeau E, Bernatchez L, Wellenreuther M (2020) Balancing selection via life-history trade-offs maintains an inversion polymorphism in a seaweed fly. *Nat Commun* 11: 670

Møller K, Langkjaer RB, Nielsen J, Piškur J, Olsson L (2004) Pyruvate decarboxylases from the petite-negative yeast Saccharomyces kluyveri. *Mol Genet Genomics* 270: 558–568

Molofsky J, Bever JD (2002) A novel theory to explain species diversity in landscapes: positive frequency dependence and habitat suitability. *Proc Biol Sci* 269: 2389–2393

Molofsky J, Bever JD, Antonovics J (2001) Coexistence under positive frequency dependence. *Proc Biol Sci* 268: 273–277

Moore FB-G, Rozen DE, Lenski RE (2000) Pervasive compensatory adaptation in *Escherichia coli*. *Proc R Soc Lond B Biol Sci* 267: 515–522

Parts L, Cubillos FA, Warringer J, Jain K, Salinas F, Bumpstead SJ, Molin M, Zia A, Simpson JT, Quail MA *et al* (2011) Revealing the genetic structure of a trait by sequencing a population under selection. *Genome Res* 21: 1131–1138

Patro R, Duggal G, Love MI, Irizarry RA, Kingsford C (2017) Salmon provides fast and bias-aware quantification of transcript expression. *Nat Methods* 14: 417–419

Peter Isabelle S, Davidson Eric H (2011) Evolution of gene regulatory networks controlling body plan development. *Cell* 144: 970–985

Pronk JT, Yde Steensma H, Van Dijken JP (1996) Pyruvate metabolism in *Saccharomyces cerevisiae*. *Yeast* 12: 1607–1633

Ratnakumar S, Hesketh A, Gkargkas K, Wilson M, Rash BM, Hayes A, Tunnacliffe A, Oliver SG (2011) Phenomic and transcriptomic analyses reveal that autophagy plays a major role in desiccation tolerance in *Saccharomyces cerevisiae*. *Mol Biosyst* 7: 139–149

Rendueles O, Amherd M, Velicer Gregory J (2015) Positively frequency-dependent interference competition maintains diversity and pervades a natural population of cooperative microbes. *Curr Biol* 25: 1673–1681

Reuß O, Vik Å, Kolter R, Morschhäuser J (2004) The SAT1 flipper, an optimized tool for gene disruption in *Candida albicans*. *Gene* 341: 119–127

Rojas Echenique JI, Kryazhimskiy S, Nguyen Ba AN, Desai MM (2019) Modular epistasis and the compensatory evolution of gene deletion mutants. *PLoS Genet* 15: e1007958

Romero IG, Ruvinsky I, Gilad Y (2012) Comparative studies of gene expression and the evolution of gene regulation. *Nat Rev Genet* 13: 505–516

Sambrook J (2001) *Molecular cloning: a laboratory manual*, 3rd edn. Cold Spring Harbor, NY: Cold Spring Harbor Laboratory Press

Scannell DR, Wolfe K (2004) Rewiring the transcriptional regulatory circuits of cells. *Genome Biol* 5: 206

Schneider CA, Rasband WS, Eliceiri KW (2012) NIH image to ImageJ: 25 years of image analysis. *Nat Methods* 9: 671–675

Segrè D, DeLuna A, Church GM, Kishony R (2005) Modular epistasis in yeast metabolism. *Nat Genet* 37: 77–83

Serrano R, Martín H, Casamayor A, Ariño J (2006) Signaling alkaline pH stress in the yeast *Saccharomyces cerevisiae* through the Wsc1 cell surface sensor and the Slt2 MAPK pathway. *J Biol Chem* 281: 39785–39795

Shevchuk NA, Bryksin AV, Nusinovich YA, Cabello FC, Sutherland M, Ladisch S (2004) Construction of long DNA molecules using long PCR-based fusion of several fragments simultaneously. *Nucleic Acids Res* 32: e19

Shi X, Ng DWK, Zhang C, Comai L, Ye W, Jeffrey Chen Z (2012) Cis- and trans-regulatory divergence between progenitor species determines gene-expression novelty in Arabidopsis allopolyploids. *Nat Commun* 3: 950

Signor SA, Nuzhdin SV (2018) The evolution of gene expression in cis and trans. *Trends Genet* 34: 532–544

Signor SA, Nuzhdin SV (2019) Compensatory evolution of gene expression. *Trends Genet* 35: 890–891

Sigwalt A, Caradec C, Brion C, Hou J, de Montigny J, Jung P, Fischer G, Llorente B, Friedrich A, Schacherer J (2016) Dissection of quantitative traits by bulk segregant mapping in a protoploid yeast species. *FEMS Yeast Res* 16: fow056

Slattery MG, Liko D, Heideman W (2006) The function and properties of the Azf1 transcriptional regulator change with growth conditions in *Saccharomyces cerevisiae*. *Eukaryot Cell* 5: 313–320

Smirnova GV, Krasnykh TA, Oktyabrsky ON (2001) Role of glutathione in the response of *Escherichia coli* to osmotic stress. *Biochemistry (Moscow)* 66: 973–978

Solís Eric J, Pandey Jai P, Zheng X, Jin Dexter X, Gupta Piyush B, Airoldi Edoardo M, Pincus D, Denic V (2016) Defining the essential function of yeast Hsf1 reveals a compact transcriptional program for maintaining eukaryotic Proteostasis. *Mol Cell* 63: 60–71

Soneson C, Love MI, Robinson MD (2015) Differential analyses for RNA-seq: transcript-level estimates improve gene-level inferences. *F1000Res* 4: 1521

Sorger PK (1990) Yeast heat shock factor contains separable transient and sustained response transcriptional activators. *Cell* 62: 793–805

Stanley D, Bandara A, Fraser S, Chambers PJ, Stanley GA (2010) The ethanol stress response and ethanol tolerance of *Saccharomyces cerevisiae*. *J Appl Microbiol* 109: 13–24

Stein T, Kricke J, Becher D, Lisowsky T (1998) Azf1p is a nuclear-localized zinc-finger protein that is preferentially expressed under non-fermentative growth conditions in *Saccharomyces cerevisiae*. *Curr Genet* 34: 287–296

Szamecz B, Boross G, Kalapis D, Kovács K, Fekete G, Farkas Z, Lázár V, Hrtyan M, Kemmeren P, Groot Koerkamp MJA *et al* (2014) The genomic landscape of compensatory evolution. *PLoS Biol* 12: e1001935

Tanaka K, Nakafuku M, Satoh T, Marshall MS, Gibbs JB, Matsumoto K, Kaziro Y, Toh-e A (1990) *S. cerevisiae* genes IRA1 and IRA2 encode proteins that may be functionally equivalent to mammalian ras GTPase activating protein. *Cell* 60: 803–807

Tanay A, Regev A, Shamir R (2005) Conservation and evolvability in regulatory networks: the evolution of ribosomal regulation in yeast. *Proc Natl Acad Sci USA* 102: 7203–7208

Taymaz-Nikerel H, Cankorur-Cetinkaya A, Kirdar B (2016) Genome-wide transcriptional response of *Saccharomyces cerevisiae* to stress-induced perturbations. *Front Bioeng Biotechnol* 4: 17

Tenaillon O, Rodríguez-Verdugo A, Gaut RL, McDonald P, Bennett AF, Long AD, Gaut BS (2012) The molecular diversity of adaptive convergence. *Science* 335: 457–461

Teng X, Dayhoff-Brannigan M, Cheng W-C, Gilbert Catherine E, Sing Cierra N, Diny Nicola L, Wheelan Sarah J, Dunham Maitreya J, Boeke Jef D, Pineda

Fernando J *et al* (2013) Genome-wide consequences of deleting any single gene. *Mol Cell* 52: 485–494

Tirosh I, Reikhav S, Levy AA, Barkai N (2009) A yeast hybrid provides insight into the evolution of gene expression regulation. *Science* 324: 659–662

Toda T, Uno I, Ishikawa T, Powers S, Kataoka T, Broek D, Cameron S, Broach J, Matsumoto K, Wigler M (1985) In yeast, RAS proteins are controlling elements of adenylate cyclase. *Cell* 40: 27–36

Tomishige N, Noda Y, Adachi H, Shimoi H, Takatsuki A, Yoda K (2003) Mutations that are synthetically lethal with a gas1Δ allele cause defects in the cell wall of *Saccharomyces cerevisiae*. *Mol Genet Genomics* 269: 562–573

Turcotte B, Liang XB, Robert F, Soontorngun N (2009) Transcriptional regulation of nonfermentable carbon utilization in budding yeast. *FEMS Yeast Res* 10: 2–13

Udom N, Chansongkrow P, Charoensawan V, Auesukaree C, Druzhinina IS (2019) Coordination of the Cell Wall integrity and high-Osmolarity glycerol pathways in response to ethanol stress in *Saccharomyces cerevisiae*. *Appl Environ Microbiol* 85: e00551-19

Van den Bergh B, Swings T, Fauvart M, Michiels J (2018) Experimental design, population dynamics, and diversity in microbial experimental evolution. *Microbiol Mol Biol Rev* 82: e00008-18

van Leeuwen J, Pons C, Mellor JC, Yamaguchi TN, Friesen H, Koschwanez J, Ušaj MM, Pechlaner M, Takar M, Ušaj M *et al* (2016) Exploring genetic suppression interactions on a global scale. *Science* 354: aag0839

van Leeuwen J, Boone C, Andrews BJ (2017) Mapping a diversity of genetic interactions in yeast. *Curr Opin Syst Biol* 6: 14–21

Venkataram S, Dunn B, Li Y, Agarwala A, Chang J, Ebel ER, Geiler-Samerotte K, Hérissant L, Blundell JR, Levy SF *et al* (2016) Development of a comprehensive genotype-to-fitness map of adaptation-driving mutations in yeast. *Cell* 166: 1585–1596

Veri AO, Robbins N, Cowen LE (2018) Regulation of the heat shock transcription factor Hsf1 in fungi: implications for temperature-dependent virulence traits. *FEMS Yeast Res* 18: foy041

Wagner GP, Lynch VJ (2008) The gene regulatory logic of transcription factor evolution. *Trends Ecol Evol* 23: 377–385

Wei G, Li Y, Du G, Chen J (2003) Effect of surfactants on extracellular accumulation of glutathione by *Saccharomyces cerevisiae*. *Process Biochem* 38: 1133–1138

Welch AZ, Gibney PA, Botstein D, Koshland DE (2013) TOR and RAS pathways regulate desiccation tolerance in *Saccharomyces cerevisiae*. *Mol Biol Cell* 24: 115–128

Wenger JW, Piotrowski J, Nagarajan S, Chiotti K, Sherlock G, Rosenzweig F (2011) Hunger artists: yeast adapted to carbon limitation show trade-offs under carbon sufficiency. *PLoS Genet* 7: e1002202

Wohlbach DJ, Thompson DA, Gasch AP, Regev A (2009) From elements to modules: regulatory evolution in Ascomycota fungi. *Curr Opin Genet Dev* 19: 571–578

Wünsche A, Dinh DM, Satterwhite RS, Arenas CD, Stoebel DM, Cooper TF (2017) Diminishing-returns epistasis decreases adaptability along an evolutionary trajectory. *Nat Ecol Evol* 1: 61